Version TOL/2

EGT3
ENGINEERING TRIPOS PART IIB

Tuesday 28 April 2026 9.30 to 11.10

Module 4G7

CONTROL & COMPUTATION IN LIVING SYSTEMS

*Answer **both** questions in section A. Answer **one** question in section B*

All questions carry the same number of marks.

*The **approximate** percentage of marks allocated to each part of a question is indicated in the right margin.*

Manuscripts referenced in part B are attached.

STATIONERY REQUIREMENTS
Single-sided script paper

SPECIAL REQUIREMENTS TO BE SUPPLIED FOR THIS EXAM
CUED approved calculator allowed
Attachment 1: Briat et al (2016) paper for Question 3 (12 pages)
Attachment 2: Gregor et al (2007) paper for Question 4 (12 pages)
Engineering Data Book

10 minutes reading time is allowed for this paper at the start of the exam.

You may not start to read the questions printed on the subsequent pages of this question paper until instructed to do so.

You may not remove any stationery from the Examination Room.

SECTION A

Answer **both** questions.

1 Consider a model of gene expression in which mRNA concentration (m) evolves as:

$$\dot{m} = \alpha - \beta m$$

where α and β are positive constants.

(a) Outline the assumptions underlying this model. Does it violate the Law of Mass-Action? [10%]

(b) Suppose we replace α with $f(m)$, where f is a monotonically decreasing function such that the system retains the same equilibrium.

(i) What effect does this have on the settling rate of the system? [10%]

(ii) How does this impact the sensitivity of the system to fluctuations in β? [10%]

(iii) Biologically, why might one expect β to fluctuate? [10%]

(c) Returning to the original form of the model with constant production rate, α, consider an alternative scenario in which the mRNA copy number, m, is a discrete variable and reactions are probabilistic.

(i) Write down the master equation for the resulting system. [10%]

(ii) Derive an expression for the probability, $P(m)$, of there being m molecules present at steady state in terms of $P(0)$. [20%]

(iii) Show that the steady state distribution of m is Poisson and find an expression for the mean and variance. [20%]

(iv) Provide a quantitative argument to explain why stochastic fluctuations around the steady-state mean value of m become negligible as m becomes large. [10%]

2 A population of cells in a bioreactor grows according to:

$$\dot{c} = rc(K - c) + u + d$$

where c is the density of cells, r and K are positive parameters, u is the rate at which cells are harvested and d represents external disturbances.

(a) (i) Provide a biological interpretation of the model parameters r and K. [10%]

(ii) Characterise the solutions of this system without solving the above ODE explicitly. [10%]

(iii) For $u = 0, d = 0$, sketch the bifurcation diagram of this system as the parameter K changes from positive to negative values, identifying any bifurcations that occur. [15%]

(iv) For a fixed $K > 0$, and $d = 0$, sketch the bifurcation diagram with u as a bifurcation parameter, identifying the bifurcation that occurs as well as its critical value, u_c. [15%]

(v) Suppose cells are being harvested at a constant rate, $u(t) = u < 0$, and that $d(t)$ consists of small, time-varying random fluctuations. Using appropriate sketches and clear reasoning, describe the effect these fluctuations have on the cell density, $c(t)$, as u is varied in a range approaching the value u_c calculated in part (iv). [20%]

(b) An integral feedback controller with gain, M, is implemented in a linear model, G, of the bioreactor to counteract the disturbances, d, and maintain the system at the nonzero equilibrium point corresponding to $u = d = 0$.

(i) Draw a block diagram of the system. [10%]

(ii) Linearise the system at its equilibrium to obtain G. [10%]

(iii) Calculate the closed loop transfer function from d to c. [10%]

SECTION B

Answer **one** question.

3 Refer to the attached paper by Briat et al (2016).

(a) Summarise the aim, approach, assumptions and findings of the paper in no more than 600 words. You may use diagrams if you wish. [60%]

(b) Show that the model system in Figure 4A of Briat et al has a unique fixed point and find conditions for the stability of the fixed point when $\eta = k = 1$ and $\mu = 2$. You may make use of (a special case of) the Routh-Hurwitz criterion, stated below. [40%]

The Routh-Hurwitz criterion for the polynomial:

$$p(s) = a_4 s^4 + a_3 s^3 + a_2 s^2 + a_1 s^1 + a_0.$$

Suppose $a_0, ..., a_4 > 0$. Then the roots of $p(s)$ lie in the left half plane if and only if

$$a_1 a_2 a_3 > a_1^2 a_4 + a_3^2 a_0.$$

4 Refer to the attached paper by Gregor et al (2007).

(a) Summarise the aim, approach, assumptions and findings of the paper in no more than 600 words. You may use diagrams if you wish. [60%]

(b) Nuclei in the *Drosophila* embryo are not separated by cell membranes and instead exist together in a cytoplasmic gel called a syncytium. Based on the reasoning in the paper, how would the presence of cell membranes affect morphogen sensing in the embryo? [40%]

END OF PAPER

Cell Systems
Article

Antithetic Integral Feedback Ensures Robust Perfect Adaptation in Noisy Biomolecular Networks

Corentin Briat,[1,2] Ankit Gupta,[1,2] and Mustafa Khammash[1,*]
[1]Department of Biosystems Science and Engineering (D-BSSE), ETH–Zürich, Mattenstrasse 26, 4058 Basel, Switzerland
[2]Co-first author
*Correspondence: mustafa.khammash@bsse.ethz.ch
http://dx.doi.org/10.1016/j.cels.2016.01.004

SUMMARY

The ability to adapt to stimuli is a defining feature of many biological systems and critical to maintaining homeostasis. While it is well appreciated that negative feedback can be used to achieve homeostasis when networks behave deterministically, the effect of noise on their regulatory function is not understood. Here, we combine probability and control theory to develop a theory of biological regulation that explicitly takes into account the noisy nature of biochemical reactions. We introduce tools for the analysis and design of robust homeostatic circuits and propose a new regulation motif, which we call antithetic integral feedback. This motif exploits stochastic noise, allowing it to achieve precise regulation in scenarios where similar deterministic regulation fails. Specifically, antithetic integral feedback preserves the stability of the overall network, steers the population of any regulated species to a desired set point, and adapts perfectly. We suggest that this motif may be prevalent in endogenous biological circuits and useful when creating synthetic circuits.

INTRODUCTION

Perfect adaptation is that property of a biological system (e.g., a cell) that enables it to adapt after an external stimulus and maintain responsiveness to further stimuli. This is usually accomplished by returning to a pre-established baseline; a new balance of components or activities is established within the system to maintain that baseline in the presence of the stimulus. Such a balancing tendency is called homeostasis. The ability to maintain homeostasis is a defining feature of many biological systems (e.g., the maintenance of plasma calcium concentration in mammals, the level of excitability in neurons, and internal pressure in various cells). While the mechanisms used to maintain homeostasis are often uncharacterized and likely diverse, they must share certain properties if adaptation is to be perfect. Notably, to be effective, an adaptation mechanism must be robust: that is, it must remain functional over a wide range of stimulus levels and be insensitive to variations in the biochemical parameters of the network.

A central strategy for realizing robust perfect adaptation is to use integral feedback. Roughly speaking, a system that implements integral feedback does two things. First, it measures a quantity that reflects some undesirable imbalance (e.g., deviation from baseline) by integrating that quantity over time. Second, it uses the result of that integration to drive processes that correct the imbalance and drive it to zero (i.e., it engages negative feedback). These behaviors are present in biological systems. For example, in Barkai and Leibler (1997) and Alon et al. (1999), it was observed that the bacterial chemotaxis network achieves adaptation to attractant signals and that the precision of this adaptation is robust to changes in the concentration of the network's proteins. It was subsequently inferred by Yi et al. (2000) that robust perfect adaptation in bacterial chemotaxis is achieved through integral feedback. While bacterial chemotaxis provides one example of a network that can realize integral feedback control, other systems with different network structures have also been shown to utilize integral feedback for achieving robust perfect adaptation. For example, in *Saccharomyces cerevisiae*, nuclear enrichment of the MAP kinase Hog1 adapts perfectly to changes in external osmolarity following an osmotic shock (Muzzey et al., 2009). This adaptation requires Hog1 kinase activity (Muzzey et al., 2009), and together these observations reveal the presence of an uncharacterized integral feedback action that is dependent on the Hog1-containing MAP kinase cascade. At the level of organ systems, we have demonstrated that calcium homeostasis in mammals relies on an integral feedback strategy to achieve robust perfect adaptation following changes in blood plasma calcium clearance or influx (El-Samad et al., 2002). This ability to maintain homeostasis is biologically important: it allows mammals to maintain physiological concentrations of blood plasma calcium within tight tolerances, despite the fact that demands for calcium vary substantially over time. Other motifs ensuring robust perfect adaptation in biochemical networks have also been reported (Ma et al., 2009; Shinar and Feinberg, 2010), and their connection to integral feedback control is currently a topic of research.

In engineering applications, integral feedback is recognized as a principal strategy for homeostatic-type regulation (for a primer, see Box 1). The Proportional-Integral-Derivative (PID) control architecture, which includes integral feedback as an essential element, is a workhorse of industrial control systems and is implemented in the majority of all automatic control applications (Åström and Hägglund, 1995). Undoubtedly, the prevalence of such a control strategy in natural and man-made systems is due to a well-described, inherent property of integral feedback: it can robustly steer a regulated system variable to a desired

Box 1. Elements of Feedback Control Systems: A Primer

Feedback control systems are workhorses of modern technology. They are also prevalent at every level of biological organization. Control theory deals with the analysis and the design of such systems. We outline the key elements of feedback control systems using a familiar example—a modern airplane. The goal of every feedback control system is to regulate the behavior of a given dynamical system (we refer to this as "the controlled system"). Regulation is achieved by manipulating a variable of the system (we refer to this as "the actuated variable"), which, in turn, affects the system dynamics. The actuated variable is manipulated according to a goal: the system output (which we refer to as "the regulated variable") should follow a desired behavior. In the case of our airplane example (see Box 1 figure, left), the actuated variable is the deflection angle of the elevator, while the regulated variable is the airplane altitude. The control objective is to have the regulated variable reach a desired altitude (we refer to this as the "set point") and to remain there in stable balance over time (we refer to this as "set-point tracking"), in spite of external factors like wind drift (we refer to these as "disturbances") that tend to drive the system into imbalance.

Manipulating the actuated variable to achieve set-point tracking is the task of the "feedback control system." This system can be physically built (in real-world applications) or can be inferred to exist based on systems-level behaviors observed during experiments (in biology). We focus on real-world examples here. The control system takes as its input a continuous measurement of a dynamic variable that gives information about the regulated variable (we refer to this as "the measured variable"; it happens to be equal to the regulated variable in our airplane example). Information from the measured variable is processed in the control system, along with the desired set point, to generate a correction signal (we refer to this signal as "the control signal") that is fed back to the controlled system, thereby "closing the loop." For example, the control signal in our example is the electronic signal that actuates the hydraulics responsible for deflecting the elevators of the airplane. There are various possible strategies that could be employed by the control system. In an integral feedback-based strategy, the control system calculates the integral, with respect to time, of the difference between the set point and the regulated variable and incorporates that into the control signal. This gives the integral feedback control strategy its name.

Importantly, this system actually contains two systems: the control system itself and the controlled system. The control system has its own dynamics, and, together with the dynamics of the controlled system, they form the aggregate dynamics of the closed-loop system, which has new properties that reflect the tight coupling of both. When coupling the dynamics of two systems through feedback, one of the key requirements is the dynamic stability of the new closed-loop system (we term this "closed-loop stability", see Box 1 figure, right). The stability of each system in isolation does not guarantee the stability of the closed loop, and one must carefully design the control system to achieve closed-loop stability. Once stability is assured, one can begin to explore the robust set-point tracking property of the system. Mathematically, set-point tracking is achieved when: $e(t) \rightarrow 0$ as $t \rightarrow \infty$, where $e(t)$ is the error signal, defined as the difference between the desired set point, r, and the controlled output $y(t)$. The above condition assures that the controlled variable tracks the desired set point after some time has elapsed.

Achieving such set-point tracking performance in spite of unknown disturbances and unknown dynamics of the controlled system is referred to as "robust set-point tracking" and is an important goal of many control systems. Control theory stipulates that control systems with certain structural properties, such as integral feedback, will achieve set-point tracking, and that tracking will be maintained regardless of system parameters and constant disturbances (provided stability is preserved). These ideas are explored more fully in Åström and Murray (2008) and Franklin et al. (2014).

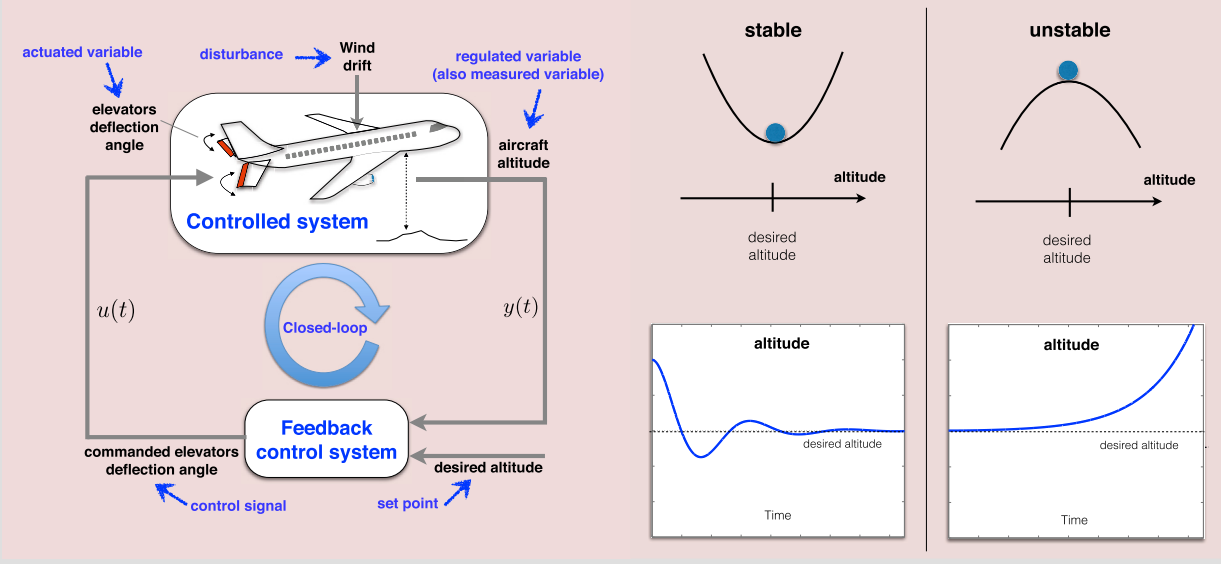

set point, while achieving perfect adaptation to disturbances (or stimuli), regardless of the model parameters (Yi et al., 2000; Åström and Murray, 2008; Francis and Wonham, 1976).

Engineered biological circuits that display perfect adaptation are rare, and current synthetic circuits only rely on simpler feedback strategies. For example, several such biochemical networks have been employed to maintain an upward bound on the level of biofuel production in bacteria (Dunlop et al., 2010). These networks were theoretically analyzed by Dunlop and colleagues, revealing that synthetic feedback loops could be used to optimize biofuel production while maintaining a low biofuel toxicity. However, the type of controllers used in Dunlop et al. (2010) did not ensure robust perfect adaptation and remained sensitive to model uncertainties. Similarly, synthetic negative feedback loops have been designed to control the translation rates of specific proteins in mammalian cells, with the goal of tuning the expression levels of multiple proteins in concert (Stapleton et al., 2012). Instead of integral feedback strategies, these engineered circuits relied on simpler feedback strategies: the strength of negative feedback is proportional to the deviation from the desired equilibrium—not the time integral of that deviation, as it is in integral feedback. While systems employing such a strategy will exhibit some amount of adaptation to constant disturbances, this adaptation is neither perfect nor robust. Instead, a constant deviation from the desired equilibrium will persist, and the amount of this deviation will depend on both the system parameters as well as the size and type of the disturbance. Consequently, these synthetic circuits require a cumbersome tuning of parameters to achieve their goals. Such tuning is difficult to realize in a biological setting (Dunlop et al., 2010). This suggests a need for synthetic circuits that are both simple and employ integral feedback in order to achieve robust perfect adaptation.

In the noise-free (deterministic) setting, integral feedback control is well understood (Åström and Hägglund, 1995) and is usually implemented in engineering applications in a configuration similar to that shown in Box 1, using flight control as an example. While the scale and exact implementation of a control strategy may change drastically, all deterministic systems (including biological ones) employing integral feedback in stable feedback loops are guaranteed to achieve robust perfect adaptation. However, in spite of our relatively good understanding of robust perfect adaptation in noise-free contexts and the role of integral feedback in achieving it, determining what constitutes integral feedback in biologically important settings, where the dynamics are described by stochastic processes, remains unclear. Moreover, strategies that are analogous to integral feedback control in intrinsically noisy cellular environments are unknown.

As in the deterministic case, a "stochastic integral feedback" strategy must achieve three goals if effective homeostasis is to be maintained. First, the overall system must have a property called "closed-loop ergodicity," meaning that the joint probability distribution of the random state vector representing the abundances of the species present in the system converges with time to a unique stationary distribution, irrespective of the initial abundances. This is somewhat analogous to the deterministic case where the trajectories of system variables (e.g., concentrations) of a closed-loop stable system converge to a set of stable equilibria regardless of their initial conditions. Second, it must display robust set-point tracking; that is, some statistic that describes a variable of interest (e.g., its mean) reaches a desired value (that is, a "set point") in a manner that is insensitive to system parameters, except those defining the set point itself. Third, it must achieve robust perfect adaptation to external disturbances. Unlike the deterministic setting, however, set-point tracking and adaptation robustness must be maintained not only with respect to model parameters, like biochemical rate constants, but also in the presence of stochastic fluctuations in species abundances.

To better understand how biology may achieve stochastic integral feedback, one can try to engineer biochemical circuits with these goals in mind. For example, one could use statistical moments (such as the mean or the variance) to describe the process to be regulated, and then to design feedback regulation strategies that steer these moments to desired values while achieving perfect adaptation (Milias-Argeitis et al., 2011). While this approach brings the problem back to the deterministic domain (statistical moments evolve according to deterministic dynamics), one is immediately faced with the so-called "moment closure problem," whereby an infinite set of deterministic differential equations is needed to determine even the first two moments (Hespanha, 2008). Similar difficulties arise if one works with the chemical master equation (see, e.g., Gillespie, 1997).

Here, we introduce an integral feedback strategy that we call antithetic integral feedback, which exhibits robust set-point tracking and robust perfect adaptation in the stochastic setting. Rather than dealing with the deterministic moments dynamics, we work with the stochastic chemical reaction network directly, thereby circumventing the moment closure problem. The objective of our control setup, represented in Figure 1A, is to bring the population average of the species $\mathbf{X}_\ell$ involved in an undefined network (the "cloud" in Figure 1A) to a desired set point. To achieve this, a new set of chemical reactions is introduced in a way that effectively implements a stochastic "antithetic integral feedback controller." For clarity, we introduce this strategy twice, once using the language of control theory, and once using more biological language.

Biological Description

The network is sensitive to $\mathbf{X}_1$, which is produced at a rate that is proportional to the amount of $\mathbf{Z}_1$. Through a network that can be arbitrarily large and uncharacterized, $\mathbf{X}_1$ activates $\mathbf{X}_\ell$. $\mathbf{Z}_2$ is produced at a rate that is proportional to the amount $\mathbf{X}_\ell$. $\mathbf{Z}_1$ and $\mathbf{Z}_2$ "annihilate" each other; however, the annihilation reaction need not result in the physical destruction of $\mathbf{Z}_1$ and $\mathbf{Z}_2$. Rather, it can be the biological activity that is abolished. For example, $\mathbf{Z}_1$ and $\mathbf{Z}_2$ may form a high-affinity, biologically inert dimer.

Regulation of *E. coli*'s sigma factor 70, σ^{70}, provides a hypothetical, concrete example of this mechanism (Figure 1B). σ^{70} is an auxiliary component of the RNA polymerase (RNAP) holoenzyme; it acts as a specificity factor and targets RNAP to the promoters of housekeeping genes. σ^{70} is regulated by a corresponding anti-sigma factor (Rsd) (Treviño-Quintanilla et al., 2013), denoted here by $\overline{\sigma}^{70}$. $\overline{\sigma}^{70}$ binds σ^{70} very tightly, sequestering it away from the RNAP core enzyme and changing the transcriptional program of the cell. Importantly, transcription of the Rsd gene is itself controlled by a σ^{70} -dependent promoter (Jishage and Ishihama, 1999); this dependence effectively closes the feedback loop that controls the activity of σ^{70}. We stress that it is yet to be experimentally verified that the σ^{70}

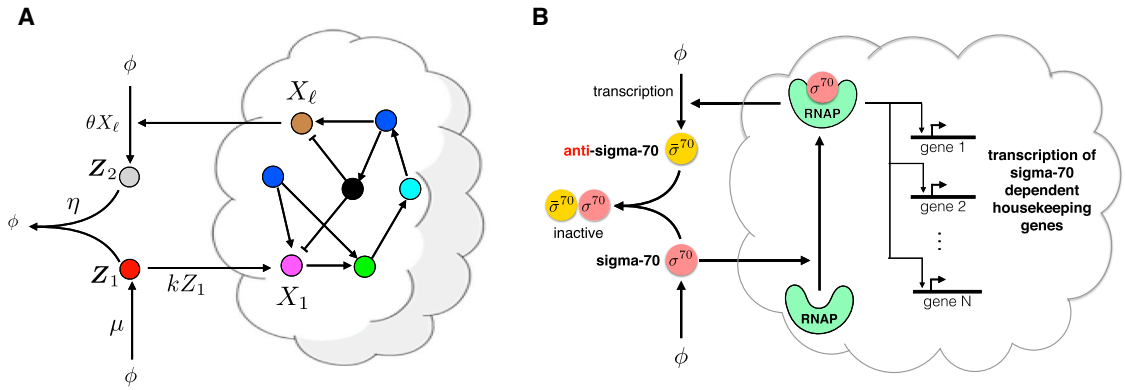

Figure 1. Antithetic Integral Feedback Controller: Generic Realization and a Specific Endogenous Example

(A) Schematic representation showing the constituents of our biomolecular control system. The network on the right (inside the cloud) represents the open-loop network, whose dynamics are to be controlled. Control is achieved by augmenting another network of reactions, referred to as the controller network (outside the cloud). Together the two networks form the closed-loop network whose dynamics are determined by the coupling resulting from the interaction of both networks. The proposed controller network, which we refer to as a "stochastic antithetic integral controller" (defined later on in Equation 1), acts on the open-loop network by influencing the rate of production of the actuated species $\mathbf{X}_1$ by means of the control input species $\mathbf{Z}_1$. The regulated species $\mathbf{X}_\ell$ will be influenced by the increase or decrease of the actuated species $\mathbf{X}_1$ and, in return, will influence the rate of production of the sensing species $\mathbf{Z}_2$, that will, finally, annihilate with the control input species $\mathbf{Z}_1$, thereby implementing a negative feedback control loop. The integral action is encoded in all the reactions of the controller network. (B) Regulation of the housekeeping genes in *E. coli*. An endogenous circuit that may employ the control strategy proposed in this article is the $\boldsymbol{\sigma}^{70}$ regulation circuit. The sigma factor $\boldsymbol{\sigma}^{70}$ binds RNA polymerase core in a complex that controls the expression of housekeeping genes during exponential growth conditions. The anti- $\boldsymbol{\sigma}^{70}$ factor, Rsd, whose gene is controlled by $\boldsymbol{\sigma}^{70}$, binds with a very strong affinity to $\boldsymbol{\sigma}^{70}$, sequestering it away from RNA polymerase. According to the theory put forth in this article, both interactions result in the tight regulation of the concentration of the **RNAP** : $\boldsymbol{\sigma}^{70}$ complex through negative feedback. While the average abundance of RNA polymerase is about 4,600 molecules per cell (Bakshi et al., 2012), the average abundance of the complex **RNAP** : $\boldsymbol{\sigma}^{70}$ (regulated species) is approximately 700 molecules per cell (Jishage and Ishihama, 1999). At the same time, the abundance of *free-* $\boldsymbol{\sigma}^{70}$ is computed to be fewer than one molecule per cell.

system in *E. coli* functions as a stochastic antithetic integral feedback controller. We simply present this as a plausible example here to facilitate understanding. (It is explored more fully in Discussion.)

Control-Theoretic Description

Our controller network consists of four reactions and two additional controller species ($\mathbf{Z}_1$ and $\mathbf{Z}_2$) that can annihilate each other. The species $\mathbf{Z}_1$ actuates the network through $\mathbf{X}_1$ which, in turn, influences the production of $\mathbf{Z}_2$ through the output species $\mathbf{X}_\ell$.

In the analysis of the stochastic antithetic integral feedback controller presented here, we demonstrate that, for a large class of networks, the steady-state value for the population average of $\mathbf{X}_\ell$ depends exclusively on the ratio of two of the controller parameters, and is independent of the network parameters. In this respect, the closed-loop network exhibits stability, robust set-point tracking, and robust perfect adaptation with respect to $\mathbf{X}_\ell$. To analyze such stochastic systems and to guarantee that they achieve these objectives, a new theory is needed. We develop such a theory here and use it to characterize a large class of networks for which we rigorously prove that our proposed controller motif indeed achieves closed-loop ergodicity, robust set-point tracking, and robust perfect adaptation—at the population level and also, in a time-averaged sense, at the single-cell level. Notably, for the class of networks considered our motif requires no specific knowledge of implementation of the biochemical network's structure or parameters. Our "stochastic antithetic integral control motif" can provably achieve all the desired properties mentioned above, even when very low molecular copy numbers exist anywhere in the network. This presents a clear advantage in synthetic biology applications, where synthetic control loops involving large molecular counts can impose a debilitating metabolic load on the cell. Our control scheme can also be shown to possess stabilizing properties that are not found in deterministic implementations of the same circuit. This provides a clear example where the intrinsic stochastic noise is beneficial—it stabilizes a system that would otherwise be unstable. This beneficial effect of noise, in the context of control theory, joins several other recent examples from the literature of noise's constructive functions including stochastic focusing (Paulsson et al., 2000), noise-induced oscillators (Vilar et al., 2002), and noise-induced switches (Tian and Burrage, 2006; Acar et al., 2008).

RESULTS

In what follows, we elaborate on the control problem under consideration, the proposed controller, along with some technical results stating the conditions under which the proposed controller solves the considered control problem. Interestingly, these conditions obtained from probability theory connect to well-known concepts of control theory, such as stability and controllability. Some additional properties, such as robustness and innocuousness, are also discussed.

The Network to Be Controlled: Open-Loop Network

We start by describing the reaction network we aim to control. Consider a reaction network with mass-action kinetics involving d molecular species denoted by $\mathbf{X}_1, \ldots, \mathbf{X}_\mathbf{d}$. Under the

well-mixedness assumption (Anderson and Kurtz, 2011), we can model the dynamics by a Markov process whose state at any given time is simply the vector of molecular counts of the d species. The "Markovian" assumption on the dynamics means that given the current state of the system, the future evolution of the state is independent of the past (memoryless property). The state evolution is influenced by K reaction channels: if the state is x, then the k-th reaction fires at rate $\lambda_k(x)$, and it displaces the state by the "stoichiometric vector" $\zeta_k \in \mathbb{Z}^d$, where $\mathbb{Z}$ denotes the set of integers. Here, λ_k is called the "propensity function" of the k-th reaction and is assumed to satisfy the property that if for any $x \in \mathbb{N}_0^d$ we have $x + \zeta_k \notin \mathbb{N}_0^d$, then $\lambda_k(x) = 0$, where $\mathbb{N}_0$ denotes the nonnegative integers. This property ensures that molecular counts of all the species remain nonnegative throughout the dynamics. In the following, we shall refer to this network as the "open-loop reaction network" and denote it by $(\mathbf{X}, \lambda, \zeta)$.

We now fix a state-space $\mathcal{S}$ for the Markovian reaction dynamics. This set $\mathcal{S}$ is a non-empty subset of $\mathbb{N}_0^d$ which is closed under the reaction dynamics. This means that for any state $x \in \mathcal{S}$ we must also have $(x + \zeta_k) \in \mathcal{S}$ if the the k-th reaction has a positive rate of firing $(\lambda_k(x) > 0)$ at state x. Selecting $\mathcal{S}$ this way allows us to use it as a generic state-space for all Markov processes describing the reaction kinetics and starting at an initial state in $\mathcal{S}$ (Gupta et al., 2014). Henceforth, we denote by $\{X(t) = (X_1(t), \ldots, X_d(t)) : t \geq 0\}$ the continuous time Markov process representing the reaction dynamics with an initial state $x_0 \in \mathcal{S}$.

From a control theoretic point of view, it is necessary to define input and output nodes of the above network. We assume here that species $\mathbf{X}_1$ is the "actuated species" that is the species that the controller can act on. The "regulated species" is $\mathbf{X}_\ell$, for some $\ell \in \{1, \ldots, d\}$, and it is the species we wish to control. The way the controller acts on the actuated species, in order to control the regulated species is depicted in Figure 1A. This will be explained in more detail in the next section.

The Control Objectives

We now state the objectives required from our control system, which includes an open-loop network and a controller network.

Objectives

Find a controller (set of additional reactions and additional species) such that, by suitably acting on the actuated species $\boldsymbol{X}_1$, we have the following properties for the closed-loop network (defined here as the interconnection of the open-loop network $(\mathbf{X}, \lambda, \zeta)$ described above with the controller network):

1. The closed-loop network is ergodic.
2. The first and second-order moments of $X(t)$ exist and are uniformly bounded and globally converging with time to their unique stationary value.
3. We have that $\mathbb{E}[X_\ell(t)] \to \mu^*$ as $t \to \infty$ for some desired set point $\mu^* > 0$.

The first requirement is fairly standard. Indeed, ergodicity is the analog of having a globally attracting fixed point for deterministic dynamics (i.e., global stability) and is required here so that the closed-loop network is well behaved, in the sense that it reaches stationarity starting from any initial distribution. The second requirement is more specific to stochastic processes, because if only the means converge, the variance can still grow unboundedly with time, which would mean that the actual dynamics of the process (its sample paths) is not well behaved, rendering the controller of little practical utility. Finally, the third statement encapsulates our desired objective of perfect adaptation (or set-point tracking), i.e., that the population mean of the regulated species $\mathbf{X}_\ell$ approaches a fixed homeostatic value μ^*.

The Controller Reactions

We propose the following controller network (Figure 1):

$$\underbrace{\varnothing \xrightarrow{\mu} \mathbf{Z}_1}_{\text{reference}}, \quad \underbrace{\varnothing \xrightarrow{\theta X_\ell} \mathbf{Z}_2}_{\text{measurement}}, \quad \underbrace{\mathbf{Z}_1 + \mathbf{Z}_2 \xrightarrow{\eta} \varnothing}_{\text{comparison}}, \quad \underbrace{\varnothing \xrightarrow{kZ_1} \mathbf{X}_1}_{\text{actuation}}, \qquad \text{(Equation 1)}$$

where $\mathbf{X}_\ell$ is the species *measured* by the controller, which is identical to the regulated species in the current setup. The species $\mathbf{Z}_1$ and $\mathbf{Z}_2$ are referred to as the "controller species." Note that the topology of the controller network belongs to a family of four control topologies (see Figure S1 in the Supplemental Information) depending on respective roles of the two controller species.

Although inspired from Oishi and Klavins (2011), the above network has a different philosophy. Besides the fact that the current setting is stochastic, the main difference lies in the way the network interacts with the environment. While the goal of the previously mentioned paper was the biomolecular implementation of linear input-output systems, the goal here is to control a reaction network. In this regard, the birth reactions of $\mathbf{Z}_1$ and $\mathbf{Z}_2$ clearly differ from the way they are defined in the previously cited paper. We now clarify the role and meaning of each of the controller reactions:

1. The first reaction is the "reference reaction" (or set point), which (partially) sets the value of the reference $\mu^* = \mu/\theta$. This value is implemented as the birth rate of species $\mathbf{Z}_1$.
2. The second reaction is the "measurement reaction" and takes the form of a pure-birth reaction with a rate proportional to the current population of the regulated species $\mathbf{X}_\ell$. It is referred to as the measurement reaction as the rate of increase of the population of $\mathbf{Z}_2$ reflects the population size of $\mathbf{X}_\ell$.
3. The third reaction implements the "comparison reaction," which decrements the molecular counts of $\mathbf{Z}_1$ and $\mathbf{Z}_2$ by one each. The rate constant for this reaction is η that can be tuned. The main role of this reaction is to correlate both the populations of $\mathbf{Z}_1$ and $\mathbf{Z}_2$ and to prevent them from growing without bounds. This reaction can be viewed as a "compare and subtract operation" since, when both $\mathbf{Z}_1$ and $\mathbf{Z}_2$ have positive populations (comparison), then this reaction decreases their respective population sizes by one (subtraction), thereby preserving the difference of their population sizes.
4. The last reaction is the "actuation reaction," which implements the way the controller acts on the system, i.e., by acting on the birth rate of the actuated species $\mathbf{X}_1$. The parameter k is also a tuning parameter of the controller.

The above controller has been chosen with an implementability constraint in mind, as it is expressed as plausible reactions that may be implemented in vivo to perform in vivo control. It will be shown later that the proposed controller exhibits strong robustness properties that make its implementation much easier than other types of controllers that require the fine tuning of their reaction rates (see also Section S5.4 of the Supplemental Information). In vitro control is also possible using, for instance, DNA strand displacement (Chen et al., 2013). In silico control (Milias-Argeitis et al., 2011; Uhlendorf et al., 2012) can be considered as well, whenever the population size of regulated species $\mathbf{X}_\ell$ can be measured in real time from outside of the cell(s) using, for instance, microscopy.

Guaranteed Performance Properties of the Controlled Network

We now consider the dynamics of the "closed-loop network," which is formed by interconnecting the open-loop network $(\mathbf{X}, \lambda, \zeta)$ with the controller (Equation 1). We can represent the dynamics by a Markov process $\{(X(t), Z(t)) : t \geq 0\}$, where for each t, $X(t) = (X_1(t), \ldots, X_d(t))$ denotes the molecular counts of the d network species and $Z(t) = (Z_1(t), Z_2(t))$ denotes the molecular counts of the two controller species. Our control objective is to steer the first-order moment $\mathbb{E}[X_\ell(t)]$ corresponding to species $\mathbf{X}_\ell$ to a desired set point μ^*. The dynamics of the first-order moments $\mathbb{E}[X(t)] = (\mathbb{E}[X_1(t)], \ldots, \mathbb{E}[X_d(t)])$ and $\mathbb{E}[Z(t)] = (\mathbb{E}[Z_1(t)], \mathbb{E}[Z_2(t)])$ is described by the following system of ordinary differential equations (ODEs)

$$\begin{aligned} \frac{d\mathbb{E}[X(t)]}{dt} &= \sum_{k=1}^{K} \zeta_k \mathbb{E}\left[\lambda_k(X(t))\right] + k\mathbb{E}[Z_1(t)]e_1, \\ \frac{d\mathbb{E}[Z_1(t)]}{dt} &= \mu - \eta\mathbb{E}[Z_1(t)Z_2(t)], \\ \frac{d\mathbb{E}[Z_2(t)]}{dt} &= \theta\mathbb{E}[X_\ell(t)] - \eta\mathbb{E}[Z_1(t)Z_2(t)], \end{aligned} \qquad \text{(Equation 2)}$$

where e_1 is the d -dimensional vector whose first component is 1 and the rest are zero. Note that this system of ODEs is not *closed* because there is no equation for the dynamics of $\mathbb{E}[Z_1(t)Z_2(t)]$. Moreover, if the propensity functions λ_k's are nonlinear functions of the state variables, additional quantities whose dynamics is not captured by these equations will be encountered. Attempting to "close" this system by adding equations for the dynamics of all these additional quantities and $\mathbb{E}[Z_1(t)Z_2(t)]$ will again lead to another set of quantities with unrepresented dynamics. This is known as the "moment-closure problem" in the literature, a well-known barrier for the direct analysis and simulation of moment equations.

As stated, it is unclear why the proposed controller structure involves integral action. By subtracting the two last equations in Equation 2 and integrating, we get

$$\mathbb{E}[(Z_1 - Z_2)(t)] = \theta \int_0^t \left(\frac{\mu}{\theta} - \mathbb{E}[X_\ell(s)]\right) ds. \qquad \text{(Equation 3)}$$

In other words, the mean difference between the two controller species is proportional to the integral of the mean tracking error. Now the role of integration in achieving perfect steady-state tracking can be understood: if it can be further ensured that as $t \to \infty$, the left-hand side converges to a constant, then the integrand (the mean tracking error) will converge to zero, which is equivalent to having $\mathbb{E}[X_\ell(s)]$ converge to the set point $\mu/\theta = \mu^*$. Ensuring the convergence of the left-hand side to a constant is related to the ergodicity of the network, which we address next.

Our approach in this paper is to find conditions ensuring that the Markov process $\{(X(t), Z(t)) : t \geq 0\}$ describing the dynamics of closed-loop reaction network is ergodic. This means that starting from any initial state, the probability distribution of the state $(X(t), Z(t))$ converges to a unique stationary distribution π as $t \to \infty$. Under fairly general conditions, ergodicity also implies that first- and second-order moments of the state $(X(t), Z(t))$ converge to constant steady-state values, which can be computed by evaluating the expectation $\mathbb{E}_\pi$ with respect to the stationary distribution π. As mentioned above, this guarantees that the integrand in Equation 3 tends to zero as $t \to \infty$ and gives

$$\mathbb{E}_\pi[X_\ell] = \frac{\mu}{\theta} = \mu^*, \qquad \text{(Equation 4)}$$

where $\mathbb{E}_\pi[X_\ell] = \lim_{t\to\infty} \mathbb{E}[X_\ell(t)]$. This shows that if the closed-loop network dynamics is ergodic, then our proposed controller automatically imposes the set-point tracking property, regardless of the initial conditions or model parameters (other than μ/θ). A sudden change in these parameters will result in the same steady-state value after a transient, thereby ensuring perfect adaptation. Achieving steady-state tracking and perfect adaptation is the main rationale behind integral control. Note that these desirable controller properties are demonstrated without solving the first-order moment Equation 2, thereby circumventing the moment-closure problem mentioned earlier.

The following result, proved in Section S4.3 of the Supplemental Information, establishes conditions under which a general stochastic biochemical reaction network can be controlled using the proposed controller network.

Theorem 1: General Network Case

Consider an open-loop reaction network $(\mathbf{X}, \lambda, \zeta)$ and assume that for some given values of its parameters, and the parameters of the controller network, the closed-loop network, formed by augmenting the open-loop network with the controller reactions (Equation 1), is ergodic and has uniformly bounded first- and second-order moments. Then, asymptotic set-point tracking is achieved, i.e., $\mathbb{E}[X_\ell(t)] \to \mu/\theta$ *as* $t \to \infty$.

The main challenge in the above result lies in verifying the ergodicity of a given closed-loop network dynamics. In what follows, we provide simple conditions that allow us to check this property using efficient computational techniques, such as linear programming. This is done for two main classes of networks, namely, those consisting of *unimolecular* reactions and those consisting of *bimolecular* reactions. In the unimolecular case, for each reaction k the propensity function $\lambda_k(x)$ is an affine function of the state variable $x = (x_1, \ldots, x_d)$. Hence, we can express each $\lambda_k(x)$ as

$$\lambda_k(x) = \sum_{i=1}^{d} w_{ki}x_i + w_{k0}$$

where w_{k0} is a nonnegative constant and w_{ki}'s are some real numbers for $i=1,\ldots,d$. Define a $K\times d$ matrix W with entries w_{ki} and let S be the $d\times K$ matrix whose k-th column is the stoichiometry vector ζ_k for reaction k. Also, let w_0 be the d-dimensional vector whose k -th component is w_{k0}. Regarding each vector as a column-vector, for any state-vector x we can write

$$\sum_{k=1}^{K}\lambda_k(x)\zeta_k = SWx + Sw_0,$$

which allows us to express the first equation in Equation 2, with $Z_1(t)\equiv 0$, as

$$\frac{d\mathbb{E}[X(t)]}{dt} = SW\mathbb{E}[X(t)] + Sw_0. \qquad \text{(Equation 5)}$$

This linear system of ODEs describes how the first-order moments of the open-loop network will evolve without the control action. If the matrix SW only has eigenvalues with negative real parts (we say in this case that the matrix SW is Hurwitz stable), then this system is asymptotically stable and the first-order moment vector $\mathbb{E}[X(t)]$ converges as $t\to\infty$. To fulfill our control objective, it is necessary that this system be asymptotically stable. This is because our controller can only act positively on the open-loop network, and hence it cannot stabilize an unstable system.

Recall that $\mathcal{S}\subset\mathbb{N}_0^d$ is the state-space for the Markovian dynamics of the open-loop reaction network. This state-space is irreducible if any state in $\mathcal{S}$ can be reached from any other state in $\mathcal{S}$ by a sequence of reactions having positive propensities at all the intermediate states. A simple example is the single-species birth-death process for which from any state value we can reach any larger state value by a sequence of birth reactions and any smaller state value by a sequence of death reactions. The irreducibility of the state-space is a necessary condition for ergodicity (Meyn and Tweedie, 1993), which holds for many reaction networks in the literature; see e.g., Gupta et al. (2014). For a unimolecular open-loop network with an irreducible state-space $\mathcal{S}$, the asymptotic stability of the linear system (Equation 5) is equivalent to the ergodicity of the open-loop network.

However, in order to ensure the ergodicity of the closed-loop network, we need a couple of other conditions that are both very natural for our control problem. The first condition is that the open-loop system be output controllable (Ogata, 1970), which simply means, in our case, that the molecular count of the regulated species $\mathbf{X}_\ell$ responds to changes in the molecular count of the actuated species $\mathbf{X}_1$. Mathematically, we can express this condition as

$$\left[(SW)^{-1}\right]_{\ell 1}\neq 0 \qquad \text{(Equation 6)}$$

where $[(SW)^{-1}]_{\ell 1}$ is the component at column 1 and row ℓ of the inverse of matrix SW. The second condition that we need is that the set point $\mu^*=\mu/\theta$ should be accessible by the dynamics of $\mathbb{E}[X_\ell(t)]$. Since our controller can only act positively on the system (Equation 5), this accessibility condition can fail if some components of the input vector Sw_0 are too large (see also the discussion below theorem S6.5 in the Supplemental Information). Technically, we can check this accessibility condition by ensuring that there exists a positive constant c and a d-dimensional vector $v=(v_1,\ldots,v_d)$ with positive entries such that each component of the vector $v^T(SW+cI_d)$, where I_d is the $d\times d$ identity matrix, is strictly negative and

$$\mu^* = \frac{\mu}{\theta} > \frac{v^T S w_0}{c v_\ell}. \qquad \text{(Equation 7)}$$

As discussed in Gupta et al. (2014), the above condition can be checked using linear programming techniques.

The following result, proved in Section S6 of the Supplemental Information, provides conditions under which a unimolecular open-loop reaction network can be controlled using the controller network (Equation 1).

Theorem 2: Unimolecular Network Case

Suppose that the open-loop reaction network $(\mathbf{X},\lambda,\zeta)$ is unimolecular and its state-space $\mathcal{S}$ is irreducible. Furthermore, assume that the linear system (Equation 5) of ODEs is asymptotically stable (SW is Hurwitz stable) and output controllable (the condition in [Equation 6] holds), and that the desired set point μ/θ is accessible (the condition in [Equation 7] holds).

Then, for any $k,\eta>0$, the closed-loop reaction network is ergodic and asymptotic set-point tracking is achieved; i.e., $\mathbb{E}[X_\ell(t)]\to\mu/\theta$ *as* $t\to\infty$. Moreover, the steady-state values of the first-order moments $\mathbb{E}[X(t)]=(\mathbb{E}[X_1(t)],\ldots,\mathbb{E}[X_d(t)])$ and $\mathbb{E}[Z_1(t)]$ are

$$\lim_{t\to\infty}\mathbb{E}[X(t)] = \frac{\mu(SW)^{-1}e_1}{\theta\left[(SW)^{-1}\right]_{\ell 1}} \quad \textit{and} \quad \lim_{t\to\infty}\mathbb{E}[Z_1(t)] = \frac{-\mu}{\theta\left[(SW)^{-1}\right]_{\ell 1}}.$$

A more general version of this result and its extension to a class of bimolecular networks are provided in Section S6 and Section S7 of the Supplemental Information. In light of theorem 2, several favorable properties for the controller and the closed-loop network can now be highlighted and expounded.

Ergodicity, Set-Point Tracking, and Bounded First- and Second-Order Moments

These are the main properties sought in our statement of control objectives. Moreover, as stated in theorem 2, the average population sizes of species $\mathbf{X}_1,\ldots,\mathbf{X_d}$ and $\mathbf{Z}_1$, at steady state, are uniquely defined by the set point μ/θ and the parameters of the open-loop network, implying that these quantities are also regulated by our stochastic antithetic integral controller.

Robustness

Robustness is a fundamental requirement that ensures that some properties for the closed-loop network are preserved, even in the presence of model uncertainties. This concept is critical in biology as the environment is fluctuating or noisy and only poorly known models are typically available. The obtained results can automatically guarantee the preservation of all the properties stated in Theorem 2, even in such constraining conditions.

Well-Behaved Single-Cell Tracking Dynamics

Ergodicity ensures that the population average at stationarity is equal to the asymptotic value of the time average of any single-cell trajectory; see, e.g., Gupta et al. (2014). We can therefore conclude that the proposed controller

achieves two goals simultaneously, as it can ensure robust set-point tracking at both the population and single-cell levels. As a consequence, the controller will also ensure single-cell set-point tracking in the presence of cell events such as cell-division when certain conditions are met (see Section S8.5 of the Supplemental Information for more details).

Innocuousness of the Controller

An inaccurate implementation of controller parameters may sometimes lead to an unstable behavior for the closed-loop system. However, the fact that the conditions of Theorem 2 are independent of k and η tells us that the proposed controller will both preserve the ergodicity of the (possibly uncharacterized) open-loop network and ensure set-point tracking/adaptation regardless of the values of its parameters, provided that the open-loop network satisfies the conditions of Theorem 2. This property is crucial in biology, as identifying models and implementing specific reaction rates (even approximately) are difficult tasks. This peculiar and non-standard property is referred here as ''innocuousness,'' and it is illustrated in Figure 4, where the deterministic and stochastic dynamics of the same controlled networks are compared (see also Section S5.4 of the Supplemental Information).

Low Metabolic Load

Even if the controller works in the low copy-number regime, it does not necessarily imply a low metabolic load for the cell. Indeed, if there is fast creation and annihilation of the controller species $\mathbf{Z}_1$ and $\mathbf{Z}_2$, then it will result in many energy consuming futile cycles, which can impose a heavy metabolic burden on the cell, even though the dynamics is still in the low copy-number regime. However, it can be shown (see Section S5.5 of the Supplemental Information) that the power consumption at stationarity of the controller reactions, denoted by $\overline{P}$, can be expressed in the case of unimolecular networks as

$$\overline{P} = \mu(\alpha_1 + \alpha_2 + \alpha_3) + \frac{\mu}{\theta}\frac{\alpha_4}{\left|\left[(SW)^{-1}\right]_{\ell 1}\right|} \qquad \text{(Equation 8)}$$

where $\alpha_1, \alpha_2, \alpha_3$ and α_4 are (positive) weights associated with the reference, measurement, comparison, and actuation reactions, respectively, that represent the energy cost of each reaction. Interestingly, only the first three terms depend on μ while the last term depends on the ratio μ/θ and some network parameters. This last term, however, would also be present in the case of the production of $\mathbf{X}_1$ at a constitutive rate equal to $\mu/(\theta\left|e_\ell^T(SW)^{-1}e_1\right|)$ (which would lead to the same steady-state value for the controlled output, but no adaptation properties). Hence, the effective metabolic load of our controller is equal to the first three terms and is only proportional to μ. A low metabolic load can therefore be easily achieved by first setting μ to a small value and then adjusting the set-point value with θ.

Circumventing Moment Closure Difficulties

Finally, we emphasize that using the proposed approach, the moment closure problem does not arise, as the main conclusions (e.g., ergodicity, set-point tracking and robustness) directly follow from stochastic analysis tools and the structure of the controller, thereby avoiding altogether the framework of the moment equations (see Section S8.6 of the Supplemental Information).

Application to Gene Expression Control: Set-Point Tracking and Perfect Adaptation

The goal of this example is to demonstrate that set-point tracking, and perfect adaptation can be ensured with respect to any change in the parameters of the gene expression network

$$\mathbf{X}_1 \xrightarrow{\gamma_1} \varnothing, \quad \mathbf{X}_1 \xrightarrow{k_2} \mathbf{X}_1 + \mathbf{X}_2, \quad \mathbf{X}_2 \xrightarrow{\gamma_2} \varnothing \qquad \text{(Equation 9)}$$

where $\mathbf{X}_1$ denotes the mRNA and $\mathbf{X}_2$ the measured/regulated species (see Figure 2). The following result is proved in Section S8.2 of the Supplemental Information:

Proposition 3

For any positive values of the parameters $k, k_2, \gamma_1, \gamma_2, \eta, \theta$, and μ, the controlled gene expression network and is ergodic, has bounded and globally converging first- and second-order moments and

$$\mathbb{E}[X_2(t)] \to \frac{\mu}{\theta} \quad as \quad t \to \infty. \qquad \text{(Equation 10)}$$

However, when we consider a Hill-type static control scheme of the form

$$\varnothing \xrightarrow{f(X_2)} \mathbf{X}_1 \quad with \quad f(X_2) = \frac{\alpha K^n}{K^n + X_2^n} \qquad \text{(Equation 11)}$$

where K, α are positive parameters and n is a positive integer, we obtain the results depicted in Figure 3. We can see that, as opposed to the stochastic antithetic integral controller, perfect adaptation is not ensured by the Hill-type static controller. Note that, even though the comparison is only made for the gene expression network and this specific choice for the Hill-type static controller, it is provable that, in general, such controllers can not ensure perfect adaptation; see Section S8.1 of the Supplemental Information for some theoretical arguments and different control schemes.

Noise as a Stabilizing Agent: Stochastic versus Deterministic Population Control

Here, we demonstrate a striking effect of noise as an agent for dynamic stabilization at the population level. We do this by comparing the results that we obtain to those we would have obtained in the deterministic setting (see Figure 4). To this aim, we again consider the gene expression network (Equation 9), and we set $k_2 = \gamma_1 = \gamma_2 = 1$ for simplicity. We then get the deterministic model and stochastic mean model depicted in Figures 4A and 4B, respectively. It is important to emphasize that the deterministic model represents here the evolution of the mean concentration of the species over a population of deterministically behaving cells with identical initial concentrations. On the other hand, the stochastic mean model represents the evolution of the mean number of the species over a population of stochastically behaving cells with identical initial molecular counts. Note that, by virtue of the ergodicity property, the stochastic mean model will always converge to its unique steady-state value regardless of the different initial conditions for the individual cells. This property does not hold in general for a deterministic model representing the average

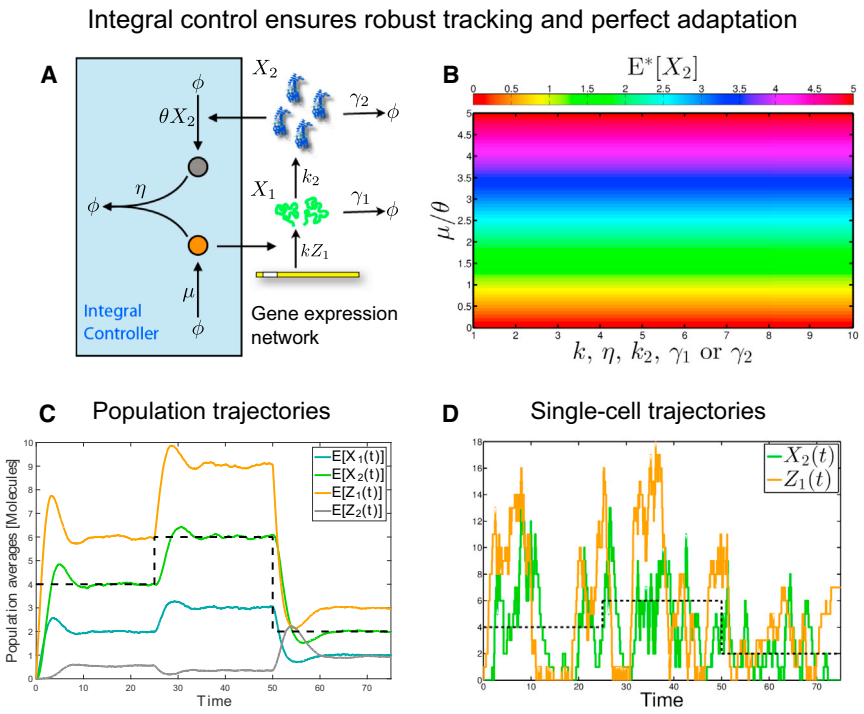

Figure 2. Stochastic Gene Expression Regulated by Antithetic Integral Controller Exhibits Tracking and Robust Perfect Adaptation

(A) The controlled gene expression network (Equation 9) with the proposed stochastic antithetic integral controller (Equation 1).

(B) The closed-loop reaction network shows perfect adaptation (at stationarity) with respect to any changes in the parameters of the network as we have that $\mathbb{E}_\pi[X_2] = \mu/\theta$ for any values of the parameters k, η, k_2, γ_1, and γ_2 where $\mathbb{E}_\pi[X_2]$ denotes the mean number of molecules of $\mathbf{X}_2$ at stationarity.

(C) The controlled-output $\mathbb{E}[X_2(t)]$ of the closed-loop network tracks the reference value (in black-dash). The mean population of input species $\mathbb{E}[Z_1(t)]$ adapts automatically to changes in the reference value $\mu^* = \mu/\theta$ without requiring re-implementation.

(D) Single-cell trajectories, although strongly affected by noise, still have an underlying regularity ensuring the convergence of the moments at the population level. All simulations have been performed using Gillespie's stochastic simulation algorithm with the parameters $k = 1$, $\gamma_1 = 3$, $k_2 = 2$, $\gamma_2 = 1$, $\theta = 1$, and $\eta = 50$.

concentrations of a population of deterministically oscillating cells. The stochastic mean model has been obtained using the identity $\mathbb{E}[Z_1Z_2] = \mathbb{E}[Z_1]\mathbb{E}[Z_2] + Cov(Z_1, Z_2)$ where the covariance term is nonzero as the random variables are not independent. If such a term would be zero, then we would recover the deterministic dynamics, but, due to noise, we can see in Figure 4C that while the deterministic dynamics may exhibit oscillations, the dynamics of the first-order moment is always globally converging to the desired steady-state value. As a final comment, we note that if we were closing the moment equations in Figure 4C by neglecting the second-order cumulant, then we would fail in predicting the correct behavior of the first-order moments. This demonstrates the central role of the noise in the stabilizing properties of the proposed stochastic antithetic integral controller. The noise can hence be viewed as here a stabilizing agent through the randomness it adds to the dynamics, allowing then for their systematic compensation at the population level, regardless of the initial conditions and the system parameters. This phenomenon is entirely due to stochasticity, and it does not generically occur in the deterministic setting.

DISCUSSION

A general control theory for stochastic biochemical reaction networks with tailored mathematical concepts and tools has been missing. We believe that a well-grounded biomolecular control theory would enable a deeper understanding of biological regulation at the molecular level. Moreover, it could pave the way for an efficient and systematic rational design of synthetic genetic circuits that steer cellular dynamics in understood ways. For such circuits, we propose the term "cybergenetic," which combines the genetic nature of the system with its cybernetic function of dynamic steering and control ("cyber" means "to steer" in Greek). In this article, we take a first step in the development of such a theory by addressing one of the central dynamic control motifs: integral feedback. The methods we developed are the product of a synthesis of ideas from control theory, probability theory, linear algebra, and optimization theory. Even though our findings are specific to the class of integral controllers we consider, they may serve as the foundation on which more general biomolecular control theory can be developed—one that deals with a larger class of stochastic dynamic controllers and networks. Indeed, numerical experiments performed on more general networks lying outside the scope of the developed theory tend to support this claim (see Section S8.7 of the Supplemental Information).

Although the proposed control motif served as a frame around which the theoretical ideas of molecular stochastic control were developed, a cybergenetic circuit implementing such a motif may be of biological significance in its own right, a possibility that we explore below for both endogenous and synthetic regulation. Indeed, the simplicity of the mechanism and the regulation properties that it confers raises the question whether such a motif could have evolved for the purpose of endogenous regulation. The species $\mathbf{Z}_1$ and $\mathbf{Z}_2$ may be RNA, protein, metabolite, or etc., but they must act to effectively "annihilate" each other. As discussed in the Introduction, this annihilation need not be physical, as long as the two species act to render each other functionless. This could occur, for example, as a result of irreversible binding of $\mathbf{Z}_1$ and $\mathbf{Z}_2$, where the new complex effectively sequesters both from performing their function.

Returning to the example of σ^{70}, $\overline{\sigma}^{70}$, and the regulation of *E. coli*'s housekeeping genes (Figure 1B), what is understood about this system's regulation fits well our antithetic integral feedback motif and suggests that the RNAP core enzyme complex with σ^{70} is the object of tight regulation. This, in turn,

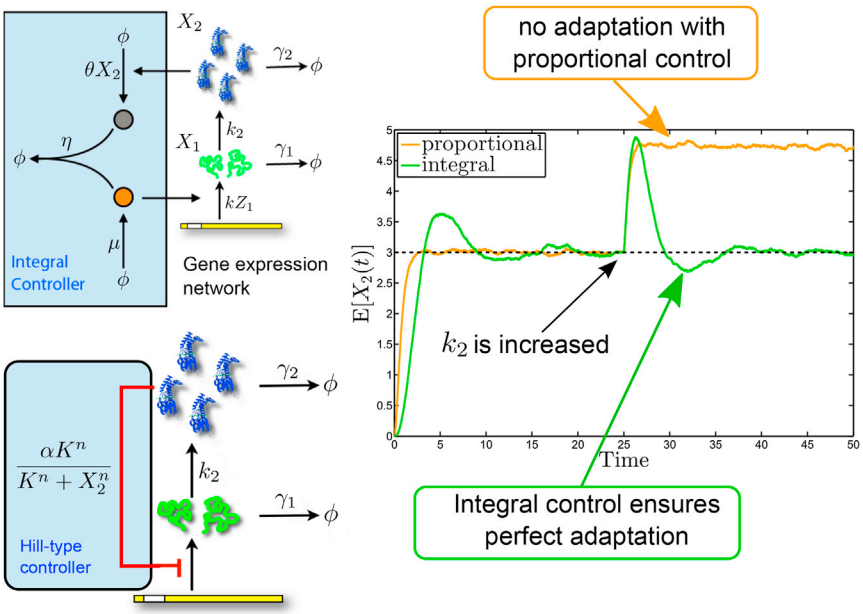

Figure 3. Comparison between Proposed Antithetic Integral Controller and Hill-type Controller

The simulation is performed using parameters initialized to $\mu = 3$, $\theta = 1$, $k = 1$, $\gamma_1 = 3$, $k_2 = 3$, $\gamma_2 = 1$ and $\eta = 50$ for the stochastic antithetic integral controller (Equation 1) and $n = 1$, $\alpha = 8.22$ and $K = 3$ for the Hill-type static controller (Equation 11). The averaging is performed over 8,000 cells simulated with Gillespie's stochastic simulation algorithm. At $t = 25$ s, the value of k_2 jumps from 3 to 6. While the proposed stochastic antithetic integral controller shows perfect adaptation, the Hill-type static controller is unable to return to the mean value of the population of $\mathbf{X}_2$ before the stimulus. This demonstrates the advantage of the integral feedback strategy over the Hill-type strategy.

suggests that the expression of all the housekeeping genes whose promoters are recognized by $\boldsymbol{\sigma}^{70}$ will be regulated in a correspondingly tight way. When binding reaction rates in the literature (Maeda et al., 2000; Bakshi et al., 2012) are used for $\boldsymbol{\sigma}^{70}$ and RNAP along with estimated average total numbers, one comes up with a very low (<1) average copy number of *free*- $\boldsymbol{\sigma}^{70}$ per cell, which would indicate that the system operates in the stochastic regime. Intriguingly, the anti- $\boldsymbol{\sigma}^{70}$ factor $\overline{\boldsymbol{\sigma}}^{70}$ is known to be involved in the transition from the log to the stationary phase of growth, during which time its concentrations are significantly elevated, leading to the downregulation of the housekeeping genes. One way to achieve this is through the increase of the rate of transcription of anti-sigma factor Rsd during transition to stationary phase, leading to the decrease in the set point for $\mathbf{RNAP} : \boldsymbol{\sigma}^{70}$ (in our analysis, this corresponds to the quantity μ/θ). Supporting this hypothesis is the fact that transcription of the $\overline{\boldsymbol{\sigma}}^{70}$ gene is known to be controlled by a $\boldsymbol{\sigma}^{38}$ -dependent promoter (Jishage and Ishihama, 1999), where $\boldsymbol{\sigma}^{38}$ is recognized as the master regulator for adaptation to stationary phase transcription. The full regulatory details of $\boldsymbol{\sigma}^{70}$ continue to unknown, and, while it remains to be experimentally verified that the $\boldsymbol{\sigma}^{70}$ and $\overline{\boldsymbol{\sigma}}^{70}$ interactions in *E. coli* function as a stochastic antithetic integral feedback controller, as put forth here, it is quite likely that these interactions play a central part in the regulation of the $\boldsymbol{\sigma}^{70}$ system, even if they do not fit the scheme proposed exactly. For example, if the expression rate of $\boldsymbol{\sigma}^{70}$, assumed here as constant, turns out to be dependent on $\mathbf{RNAP} : \boldsymbol{\sigma}^{70}$, then our analysis can be extended to show that similar regulation properties still hold. Finally, we speculate that the sigma/anti-sigma regulatory motif similar to that presented here is not uncommon in biology, as several anti-sigma factors have been found in a number of bacteria, including *E. coli* and Salmonella, as well as in the T4 bacteriophage.

Beyond endogenous circuits, our cybergenetic motif presents opportunities for applications in synthetic biology. Until now, most of the synthetic regulatory circuits have relied on proportional action—a control scheme that fails to ensure perfect adaptation in many practical situations. Moreover, existing theoretical studies of synthetic biological circuits mainly considered the deterministic setting, and hence they implicitly assumed large molecular abundances. However, the implementation of control circuits that rely on high component abundances severely impinges on the host circuit's material and energy resources, leading to increased metabolic burden that can affect both function and viability. Fortunately, this is largely avoidable, as effective control involves mostly information processing, which in principle requires little energy and material resource consumption.

The regulatory motif that we propose exhibits characteristics that provably ensure robust stability, robust set-point tracking, and robust perfect adaptation for the controlled network and is achieved with a low metabolic cost and with molecular species that can have very low abundances. It can be used for both single-cell set-point tracking (on average) and for population control. Notably, perfect adaptation will also hold in presence of static extrinsic noise (cell-to-cell variability) when understood as network parameter discrepancies. Thanks to the innocuousness of the controller, it does not need to be fine tuned and can therefore be used in many practical situations, e.g., when the controlled network is very poorly known. In this regard, the proposed controller maintains clear implementability advantages over controllers requiring parameter tuning. This latter property emerges from the random nature of the reactions, as its deterministic counterpart leads to oscillating trajectories when the controller parameters are located in a certain instability region. In spite of this, this controller can still be used in a deterministic setting even though some of the properties, such the innocuousness property, are lost. With this in mind, the proposed controller may find several applications within synthetic biology. An immediate one is the optimization of drug or fuel production in bioreactors; see, e.g., Dunlop et al. (2010). Currently, simple control strategies, such as proportional feedback or constitutive production, are used in these applications. By utilizing slightly more complex controllers, such as the one proposed here, dramatic improvements in the production process can be

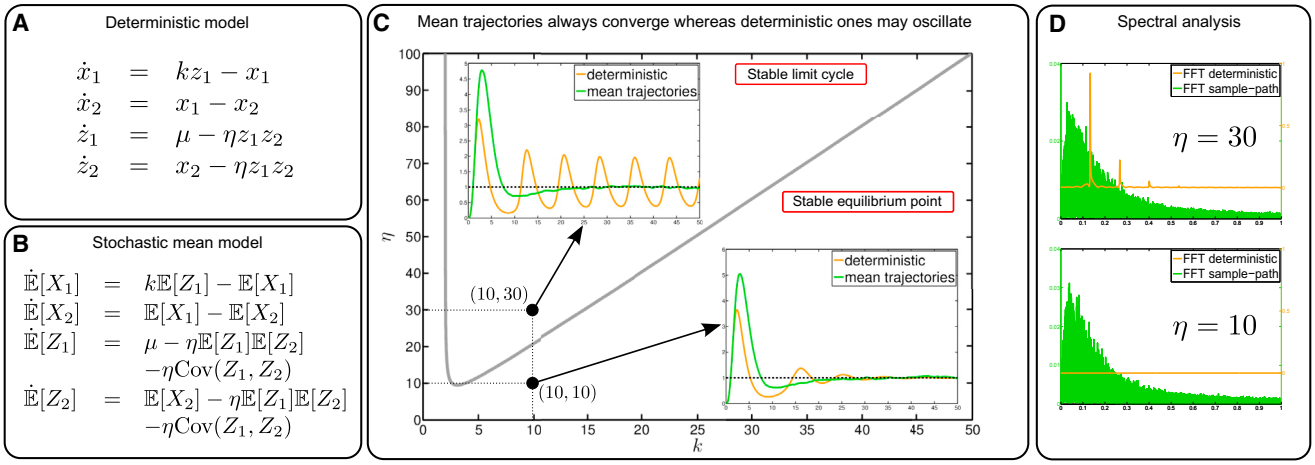

Figure 4. Antithetic Integral Feedback Controller Exploits Stochastic Noise to Achieve Robust Regulation

(A) Deterministic model for the gene expression network (Equation 9) with $k_2 = \theta = \gamma_1 = \gamma_2 = 1$.

(B) Mean model for the gene expression network (Equation 9) with $k_2 = \theta = \gamma_1 = \gamma_2 = 1$.

(C) The deterministic dynamics bifurcates from a unique stable equilibrium point when the controller parameters (k, η) are chosen below the bifurcation curve into a stable limit cycle when the controller parameters are chosen above. The first-order moments, however, always converge to the desired steady-state value for the regulated species, here $\mu = 1$, regardless of the values of the controller parameters. This can be explained by the presence of the stabilizing covariance term in the model for the stochastic means.

(D) While the frequency content at stationarity of the deterministic dynamics dramatically changes when crossing the bifurcation curve, the frequency content of the sample paths remains qualitatively the same. In this regard, the controller can be considered to perform the same way in both cases. This demonstrates the superiority and the central role of the noise in the stabilizing properties of the proposed stochastic integral controller.

expected, thanks to their enhanced robustness properties. Another important application is the design of signal insulators; see, e.g., Mishra et al. (2014), where our motif may also be applied. For example, it can be used as a buffering element in order to drive the output of a module to the input of another one. It can also be used as a constant signal generator that can be used to act on a network to be analyzed. The amplitude can be tuned by acting on the reference, which can be modified from outside the cell using light-induced techniques (Milias-Argeitis et al., 2011).

The proposed controller, however, may have some drawbacks, as it seems to introduce some additional variance to the controlled process. Even though this extra variance is not detrimental to the current control objectives, it may be a problem if the goal is to reduce the variance over a cell population. Whether the variance can be reduced via a more optimal choice of parameters or through some additional controller reactions remains a question for further research. In the end, some "extra" variance due to the controller may be unavoidable, as fundamental limitations to variance reduction with feedback (Lestas et al., 2010) are likely to hold for any molecular control circuit. Even so, controller noise should not detract from the tremendous promise of designing novel stochastic control circuits at the molecular level, where the dynamic properties, benefits, and limitations seem to be exquisitely different from those at the macroscopic scale.

SUPPLEMENTAL INFORMATION

Supplemental Information includes Supplemental Experimental Procedures and seven figures and can be found with this article online at http://dx.doi.org/10.1016/j.cels.2016.01.004.

AUTHOR CONTRIBUTIONS

Conceptualization and Methodology, C.B., A.G., and M.K.; Formal Analysis, C.B. and A.G.; Software, C.B.; Writing, C.B., A.G., and M.K.; Supervision and Funding, M.K.

ACKNOWLEDGMENTS

The authors are grateful to Adam Arkin for pointing out the similarity of the tight sigma/anti-sigma factor binding reactions to our feedback controller reactions. The authors acknowledge funding support from the Human Frontier Science Program Grant RGP0061/2011 and the Swiss National Science Foundation grant 200021-157129.

Received: June 24, 2015
Revised: November 10, 2015
Accepted: January 6, 2016
Published: January 27, 2016

REFERENCES

Acar, M., Mettetal, J.T., and van Oudenaarden, A. (2008). Stochastic switching as a survival strategy in fluctuating environments. Nat. Genet. *40*, 471–475.

Alon, U., Surette, M.G., Barkai, N., and Leibler, S. (1999). Robustness in bacterial chemotaxis. Nature *397*, 168–171.

Anderson, D., and Kurtz, T.G. (2011). Continuous time Markov chain models for chemical reaction networks. In Design and Analysis of Biomolecular Circuits: Engineering Approaches to Systems and Synthetic Biology, H. Koeppl, D. Densmore, G. Setti, and M. di Bernardo, eds. (Springer), pp. 3–42.

Åström, K.J., and Hägglund, T. (1995). PID Controllers: Theory, Design, and Tuning (Instrument Society of America).

Åström, K.J., and Murray, R.M. (2008). Feedback Systems: An Introduction for Scientists and Engineers (Princeton University Press).

Bakshi, S., Siryaporn, A., Goulian, M., and Weisshaar, J.C. (2012). Superresolution imaging of ribosomes and RNA polymerase in live Escherichia coli cells. Mol. Microbiol. *85*, 21–38.

Barkai, N., and Leibler, S. (1997). Robustness in simple biochemical networks. Nature *387*, 913–917.

Chen, Y.-J., Dalchau, N., Srinivas, N., Phillips, A., Cardelli, L., Soloveichik, D., and Seelig, G. (2013). Programmable chemical controllers made from DNA. Nat. Nanotechnol. *8*, 755–762.

Dunlop, M.J., Keasling, J.D., and Mukhopadhyay, A. (2010). A model for improving microbial biofuel production using a synthetic feedback loop. Syst. Synth. Biol. *4*, 95–104.

El-Samad, H., Goff, J.P., and Khammash, M. (2002). Calcium homeostasis and parturient hypocalcemia: an integral feedback perspective. J. Theor. Biol. *214*, 17–29.

Francis, B.A., and Wonham, W.M. (1976). The internal model principle of control theory. Automatica *12*, 457–465.

Franklin, G., Powel, J.D., and Emami-Naeinin, A. (2014). Feedback Control of Dynamic Systems, Seventh Edition (Prentice Hall).

Gillespie, D.T. (1997). A rigorous derivation of the chemical master equation. Physica A *188*, 404–425.

Gupta, A., Briat, C., and Khammash, M. (2014). A scalable computational framework for establishing long-term behavior of stochastic reaction networks. PLoS Comput. Biol. *10*, e1003669.

Hespanha, J.P. (2008). Moment closure for biochemical networks. In 3rd International Symposium on Communications, Control and Signal Processing (St. Julian's), pp. 142–147.

Jishage, M., and Ishihama, A. (1999). Transcriptional organization and in vivo role of the Escherichia coli rsd gene, encoding the regulator of RNA polymerase sigma D. J. Bacteriol. *181*, 3768–3776.

Lestas, I., Vinnicombe, G., and Paulsson, J. (2010). Fundamental limits on the suppression of molecular fluctuations. Nature *467*, 174–178.

Ma, W., Trusina, A., El-Samad, H., Lim, W.A., and Tang, C. (2009). Defining network topologies that can achieve biochemical adaptation. Cell *138*, 760–773.

Maeda, H., Fujita, N., and Ishihama, A. (2000). Competition among sevn Escherichia coliσ. Nucleic Acids Res. *28*, 3497–3503.

Meyn, S.P., and Tweedie, R.L. (1993). Stability of Markovian processes III: Foster-Lyapunov criteria for continuous-time processes. Adv. Appl. Probab. *25*, 518–548.

Milias-Argeitis, A., Summers, S., Stewart-Ornstein, J., Zuleta, I., Pincus, D., El-Samad, H., Khammash, M., and Lygeros, J. (2011). In silico feedback for in vivo regulation of a gene expression circuit. Nat. Biotechnol. *29*, 1114–1116.

Mishra, D., Rivera, P.M., Lin, A., Del Vecchio, D., and Weiss, R. (2014). A load driver device for engineering modularity in biological networks. Nat. Biotechnol. *32*, 1268–1275.

Muzzey, D., Gómez-Uribe, C.A., Mettetal, J.T., and van Oudenaarden, A. (2009). A systems-level analysis of perfect adaptation in yeast osmoregulation. Cell *138*, 160–171.

Ogata, K. (1970). Modern Control Engineering (Prentice Hall).

Oishi, K., and Klavins, E. (2011). Biomolecular implementation of linear I/O systems. IET Syst. Biol. *5*, 252–260.

Paulsson, J., Berg, O.G., and Ehrenberg, M. (2000). Stochastic focusing: fluctuation-enhanced sensitivity of intracellular regulation. Proc. Natl. Acad. Sci. USA *97*, 7148–7153.

Shinar, G., and Feinberg, M. (2010). Structural sources of robustness in biochemical reaction networks. Science *327*, 1389–1391.

Stapleton, J.A., Endo, K., Fujita, Y., Hayashi, K., Takinoue, M., Saito, H., and Inoue, T. (2012). Feedback control of protein expression in mammalian cells by tunable synthetic translational inhibition. ACS Synth. Biol. *1*, 83–88.

Tian, T., and Burrage, K. (2006). Stochastic models for regulatory networks of the genetic toggle switch. Proc. Natl. Acad. Sci. USA *103*, 8372–8377.

Treviño-Quintanilla, L.G., Freyre-González, J.A., and Martínez-Flores, I. (2013). Anti-sigma factors in e. coli: Common regulatory mechanisms controlling sigma factors availability. Curr. Genomics *14*, 378–387.

Uhlendorf, J., Miermont, A., Delaveau, T., Charvin, G., Fages, F., Bottani, S., Batt, G., Hersen, P., Batt, G., and Hersen, P. (2012). Long-term model predictive control of gene expression at the population and single-cell levels. Proc. Natl. Acad. Sci. USA *109*, 14271–14276.

Vilar, J.M.G., Kueh, H.Y., Barkai, N., and Leibler, S. (2002). Mechanisms of noise-resistance in genetic oscillators. Proc. Natl. Acad. Sci. USA *99*, 5988–5992.

Yi, T.-M., Huang, Y., Simon, M.I., and Doyle, J. (2000). Robust perfect adaptation in bacterial chemotaxis through integral feedback control. Proc. Natl. Acad. Sci. USA *97*, 4649–4653.

Cell

Probing the Limits to Positional Information

Thomas Gregor,[1,2,3,4,*] David W. Tank,[1,2,3] Eric F. Wieschaus,[2,4] and William Bialek[1,3]
[1] Joseph Henry Laboratories of Physics
[2] Department of Molecular Biology
[3] Lewis-Sigler Institute for Integrative Genomics
[4] Howard Hughes Medical Institute
Princeton University, Princeton, NJ 08544, USA
*Correspondence: tg2@princeton.edu
DOI 10.1016/j.cell.2007.05.025

SUMMARY

The reproducibility and precision of biological patterning is limited by the accuracy with which concentration profiles of morphogen molecules can be established and read out by their targets. We consider four measures of precision for the Bicoid morphogen in the *Drosophila* embryo: the concentration differences that distinguish neighboring cells, the limits set by the random arrival of Bicoid molecules at their targets (which depends on absolute concentration), the noise in readout of Bicoid by the activation of Hunchback, and the reproducibility of Bicoid concentration at corresponding positions in multiple embryos. We show, through a combination of different experiments, that all of these quantities are ~10%. This agreement among different measures of accuracy indicates that the embryo is *not* faced with noisy input signals and readout mechanisms; rather, the system exerts precise control over absolute concentrations and responds reliably to small concentration differences, approaching the limits set by basic physical principles.

INTRODUCTION

The macroscopic structural patterns of multicellular organisms have their origins in spatial patterns of morphogen molecules (Wolpert, 1969; Lawrence, 1992). Translating this qualitative picture into quantitative terms raises several difficulties. First is the problem of precision (Figure 1): Neighboring cells often adopt distinct fates, but the signals that drive these decisions involve very small differences in morphogen concentration, and these must be discriminated against the inevitable background of random noise. The second problem is reproducibility: If cells "know" their location based on the concentration of particular morphogens, then generating reproducible final patterns requires either that the absolute concentrations of these molecules be reproducible from embryo to embryo or that there exist mechanisms which achieve a robust output despite variable input signals. These problems of precision and reproducibility are potentially relevant to all biochemical and genetic networks, and analogous problems of noise (de Vries, 1956; Barlow, 1981; Bialek, 1987, 2002) and robustness (LeMasson et al., 1993; Goldman et al., 2001) have long been explored in neural systems. Here we address these issues in the context of the initial events in fruit fly development.

The primary determinant of patterning along the anterior-posterior axis in the fly *Drosophila melanogaster* is the gradient of Bicoid (Bcd), which is established by maternal placement of *bcd* mRNA at the anterior end of the embryo (Driever and N"usslein-Volhard, 1988a, 1988b); Bcd acts as a transcription factor, regulating the expression of *hunchback* (*hb*) and other downstream genes (Struhl et al., 1989; Rivera-Pomar et al., 1995; Gao and Finkelstein, 1998). This cascade of events generates a spatial pattern so precise that neighboring nuclei have readily distinguishable levels of expression for several genes (as reviewed by Gergen et al., 1986), and these patterns are reproducible from embryo to embryo (Crauk and Dostatni, 2005; Holloway et al., 2006).

In trying to quantify the precision and reproducibility of the initial events in morphogenesis, we can ask four conceptually distinct questions:

- If cells make decisions based on the concentration of Bcd alone, how accurately must they "measure" this concentration to be sure that neighboring cells reach reliably distinguishable decisions?
- What is the smallest concentration difference that can be measured reliably, given the inevitable noise that results from random arrival of individual Bcd molecules at their target sites along the genome?
- What level of precision does the system actually achieve (for example in the transformation from Bcd to Hb)?
- How reproducible are the absolute Bcd concentrations at corresponding locations in different embryos?

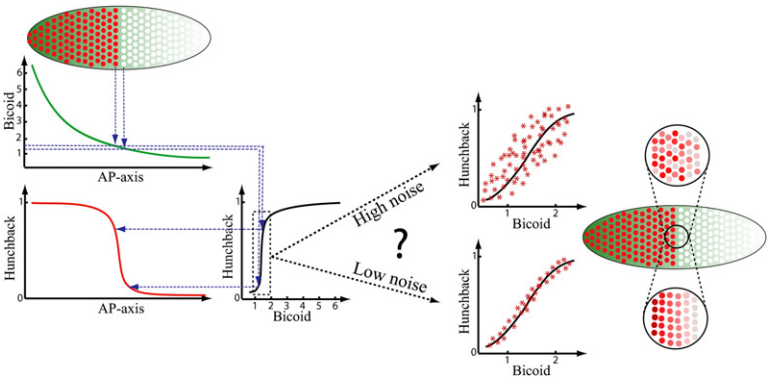

Figure 1. Schematic of the Readout Problem for the Bicoid Gradient

At left, the conventional picture. A smooth gradient of Bcd concentration is translated into a sharp boundary of Hb expression because Bcd acts as a cooperative activator of the *hb* gene. Although intended as a sketch, the different curves have been drawn to reflect what is known about the scales on which both the Bcd and Hb concentrations vary. Note that neighboring cells along the anterior-posterior axis experience Bcd concentrations that are very similar (differing by ~10%, as explained in the text), yet the resulting levels of Hb expression are very different. At right, we consider a larger number of cells in the midembryo region where Hb expression switches from high to low values. From direct experiments on simpler systems we know that, even when the concentrations of transcription factors are fixed, the resulting levels of gene expression will fluctuate (Elowitz et al., 2002; Raser and O'Shea, 2004), and there are physical limits to how much this noise can be reduced (Bialek and Setayeshgar, 2005, 2006). If the noise is low, such that a scatter plot of Hb expression versus Bcd concentration is relatively tight, then the qualitative picture of a sharp Hb expression boundary is perturbed only slightly. If the noise is large, so that there is considerable scatter in the relationship between Bcd and Hb measured for individual cells, then the sharp Hb expression boundary will exist only on average and not along individual rows in individual embryos.

The answer to the first question just depends on the spatial profile of Bicoid concentration (Houchmandzadeh et al., 2002). To answer the second question we need to know the absolute concentration of Bcd in nuclei, and we measure this using the Bcd-GFP fusion constructs described in a companion paper (Gregor et al., 2007 [this issue of *Cell*]). To answer the third question we characterize directly the input/output relation between Bcd and Hb protein levels in each nucleus of individual embryos. Finally, to answer the fourth question we make absolute concentration measurements on many embryos, as well as using more classical antibody staining methods. In the end, we find that all of these questions have the same answer: ~10% accuracy in the Bcd concentration. While this number is interesting, it is the agreement among the four different notions of precision that we find most striking.

A number of previous groups have argued that the central problem in thinking quantitatively about the early events in development is to understand how an organism makes precise patterns given sloppy initial data and noisy readout mechanisms (von Dassow et al., 2000; Houchmandzadeh et al., 2002; Spirov and Holloway, 2003; Jaeger et al., 2004; Eldar et al., 2004; Martinez Arias and Hayward, 2006; Holloway et al., 2006). In contrast, our results lead us to the problem of understanding how extreme precision and reproducibility—down to the limits set by basic physical principles—are achieved in the very first steps of pattern formation.

RESULTS

Setting the Scale

Two to three hours after fertilization of the egg, adjacent cells have adopted distinct fates, as reflected in their patterns of gene expression. At this stage, the embryo is ~500 μm long, and neighboring nuclei are separated by $\Delta x \sim 8\mu m$. Distinct fates in neighboring cells therefore means that they acquire positional information with an accuracy of ~1%–2% along the anterior-posterior axis. Measurements of Bcd concentration by immunostaining reveal an approximately exponential decay along this axis, $c(x) = c_0 \exp(-x/\lambda)$, with a length constant $\lambda \sim 100$ μm (Houchmandzadeh et al., 2002). Neighboring nuclei, at locations x and $x + \Delta x$, thus experience Bcd concentrations which differ by a fraction

$$\frac{\Delta c(x)}{c(x)} = \frac{1}{c(x)}\left|\frac{dc(x)}{dx}\right|\Delta x = \frac{\Delta x}{\lambda} \sim 0.1. \quad (1)$$

To distinguish individual nuclei from their neighbors reliably using the Bcd morphogen alone therefore would require each nucleus to "measure" the Bcd concentration with an accuracy of ~10%.

Absolute Concentrations

The difficulty of achieving precise and reproducibly functioning biochemical networks is determined in part by the absolute concentration of the relevant molecules: for sufficiently small concentrations, the randomness of individual molecular events must set a limit to precision (Berg and Purcell, 1977; Bialek and Setayeshgar, 2005, 2006). Since Bcd is a transcription factor, what matters is the concentration in the nuclei of the forming cells. A variety of experiments on Bcd (Ma et al., 1996; Burz et al., 1998; Zhao et al., 2002) and other transcription factors (Ptashne, 1992; Pedone et al., 1996; Winston et al., 1999) suggest that they are functional in the nanomolar range, but to our knowledge there exist no direct in vivo measurements in the *Drosophila* embryo.

In Figure 2A we show an optical section through a live *Drosophila* embryo that expresses a fully functional fusion of the Bcd protein with the green fluorescent protein, GFP (Gregor et al., 2007) of the native Bcd. In scanning two-photon microscope images we identify individual nuclei to measure the mean fluorescence intensity in each

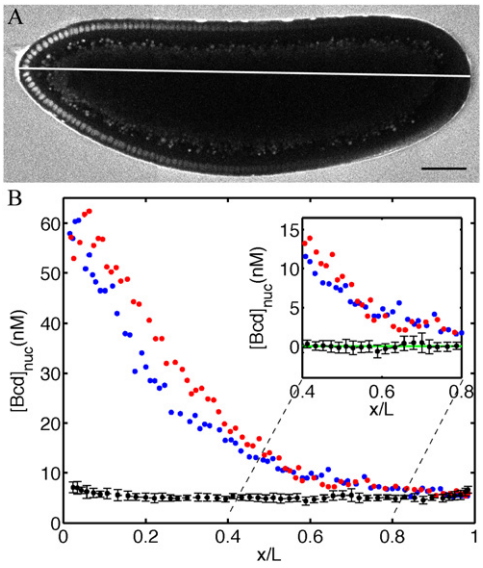

Figure 2. Absolute Concentration of Bcd

(A) Scanning two-photon microscope image of a *Drosophila* embryo expressing a Bcd-GFP fusion protein (Gregor et al., 2007); scale bar 50μm. The embryo is bathed in a solution of GFP with concentration 36 nM. We identify individual nuclei and estimate the mean Bcd-GFP concentration by the ratio of fluorescence intensity to this standard.

(B) Apparent Bcd-GFP concentrations in each visible nucleus plotted versus anterior-posterior position x (reference line in [A]) in units of the egg length L; red and blue points are dorsal and ventral, respectively. Repeating the same experiments on wild-type flies which do not express GFP, we find a background fluorescence level shown by the black points with error bars (standard deviation across four embryos). In the inset we subtract the mean background level to give our best estimate of the actual Bcd-GFP concentration in the nuclei near the midpoint of the embryo. Points with error bars show the nominal background, now at zero on average.

nucleus, which should be proportional to the protein concentration. To establish the constant of proportionality we bathe the embryo in a solution of purified GFP with known concentration and thus compare fluorescence levels of the same moiety under the same optical conditions (see Experimental Procedures).

Some of the observed fluorescence is contributed by molecules other than the Bcd-GFP, and we estimate this background by imaging wild-type embryos under exactly the same conditions. As shown in Figure 2B, this background is almost spatially constant and essentially equal to the level seen in the Bcd-GFP flies at the posterior pole, consistent with the idea that the Bcd concentration is nearly zero at this point.

Figure 2B shows the concentration of Bcd-GFP in nuclei as a function of their position along the anterior-posterior axis. The maximal concentration near the anterior pole, corrected for background, is $c_{max} = 55 \pm 3$ nM, while the concentration in nuclei near the midpoint of the embryo, near the threshold for activation of *hb* expression (at a position $x/L \sim 48\%$ from the anterior pole), is $c = 8 \pm 1$ nM. This is close to the disassociation constants measured in vitro for binding of Bcd to its target sequences in the *hb* enhancer (Ma et al., 1996; Burz et al., 1998; Zhao et al., 2002).

Physical Limits to Precision

Our interest in the precision of the readout mechanism for the Bcd gradient is heightened by the theoretical difficulty of achieving precision on the ~10% level. To begin, note that 1 nM corresponds to 0.6molecules/μm^3, so that the concentration of Bcd in nuclei near the midpoint of the embryo is $c = 4.8 \pm 0.6$ molecules/μm^3 or 690 total molecules in the nucleus during nuclear cycle 14. A 10% difference in concentration thus amounts to changes of ~70 molecules.

Berg and Purcell (1977) emphasized, in the context of bacterial chemotaxis, that the physical limit to concentration measurements is set not by the total number of available molecules but by the dynamics of their random arrival at their target locations. Consider a receptor of linear size a and assume that the receptor occupancy is integrated for a time T. Berg and Purcell argued that the precision of concentration measurements is limited to

$$\frac{\delta c}{c} \sim \frac{1}{\sqrt{DacT}}, \qquad (2)$$

where c is the concentration of the molecule to which the system is responding and D is its diffusion constant in the solution surrounding the receptor. Recent work shows that the Berg-Purcell result really is a lower limit to the noise level (Bialek and Setayeshgar, 2005, 2006): the complexities of the kinetics describing the interaction of the receptor with the signaling molecule just add extra noise but cannot reduce the effective noise level below that in Equation 2. These theoretical results encourage us to apply this formula to understand the sensitivity of cells not just to external chemical signals (as in chemotaxis) but also to internal signals, including morphogens such as Bcd.

Here we estimate the parameters that set the limiting accuracy in Equation 2; for details see Supplemental Data. The total concentration of Bcd in nuclei is $c = 4.8 \pm 0.6$ molecules/μm^3 near the point where the "decision" is made to activate Hb (Figure 2B). Bicoid diffuses slowly through the dense cytoplasm surrounding the nuclei with a diffusion constant $D < 1 \mu m^2/s$ (Gregor et al., 2007), which is similar to that observed in bacterial cells (Elowitz et al., 1999), and we take this as a reasonable estimate of the effective diffusion constant for Bcd in the nucleus. Receptor sites for eukaryotic transcription factors are ~10 base pair segments of DNA with linear dimensions $a \sim 3$ nm. The remaining parameter, which is unknown, is the amount of time T over which the system averages in determining the response to the Bcd gradient; the longer the averaging time, the lower the noise level. Putting together the parameters above, we have

$$\frac{\delta c}{c} \sim [DacT]^{-1/2} = \left[(1\mu m^2/s)(3nm)(4.8/\mu m^3)T\right]^{-1/2} \sim \left(\frac{70s}{T}\right)^{1/2}. \qquad (3)$$

Thus to achieve precision on the ~10% level (i.e., $\delta c/c \sim 0.1$) requires $T \sim 7000$ s or nearly two hours. This is almost the entire time available for development from fertilization up to cellularization, and it seems implausible that downstream gene expression levels reflect an average of local Bcd concentrations over this long time, especially given the enormous changes in local Bcd concentration during the course of each nuclear cycle (Gregor et al., 2007).

Our discussion ignores all noise sources other than the fundamental physical process of random molecular arrivals at the relevant binding sites; additional noise sources would necessitate even longer averaging times. Although there are uncertainties, the minimum time required to push the physical limits down to the ~10% level seems inconsistent with the pace of developmental events.

Input/Output Relations and Noise

The fact that neighboring cells can generate distinct patterns of gene expression does not mean that any single step in the readout of the primary morphogen gradients achieves this level of precision. Here we measure more directly the precision of the transformation from Bcd to Hb, one of the first steps in the generation of anterior-posterior pattern.

In Figure 3A we show confocal microscope images of a *Drosophila* embryo fixed during nuclear cycle 14 and immunostained for DNA, Bcd, and Hb; the fluorescence peaks of the different labels are sufficiently distinct that we can obtain independent images of the three stains. The DNA images allow us to locate automatically the centers and outlines of the ~1200 nuclei in a single image of one embryo (see Experimental Procedures). Given these outlines we can measure the average intensity of Bcd and Hb staining in each nucleus (Figure 3B). We have shown in a companion paper (Gregor et al., 2007) that immunofluorescent staining intensity I is proportional to protein concentration c plus some nonspecific background, $I = Ac + B$, where A and B are constant in a single image. With this linearity, a single image provides more than 1000 points on the scatter plot of Hb expression level versus Bcd concentration, as in Figure 3C.

Scatter plots as in Figure 3 contain information both about the mean "input/output" relation between Bcd and Hb and about the precision or reliability of this response. We can think of these data as the generalization to multicellular, eukaryotic systems of the input/output scatter plots measured for engineered regulatory elements in bacteria (e.g., Figure 3B of Rosenfeld et al., [2005]). To analyze these data we discretize the Bcd axis into bins, grouping together nuclei which have very similar levels of staining for Bcd; within each bin we compute the mean and variance of the Hb intensity. We measure the Hb level in units of its maximal mean response and the Bcd level in units of the level which generates (on average) half-maximal Hb.

Input/output relations between Bcd and Hb are shown for nine individual embryos in Figure 4A. Results from different embryos are very similar (see Experimental Procedures for discussion of normalization across embryos), and pooling the results from all embryos yields an input/output relation that fits well to the Hill relation,

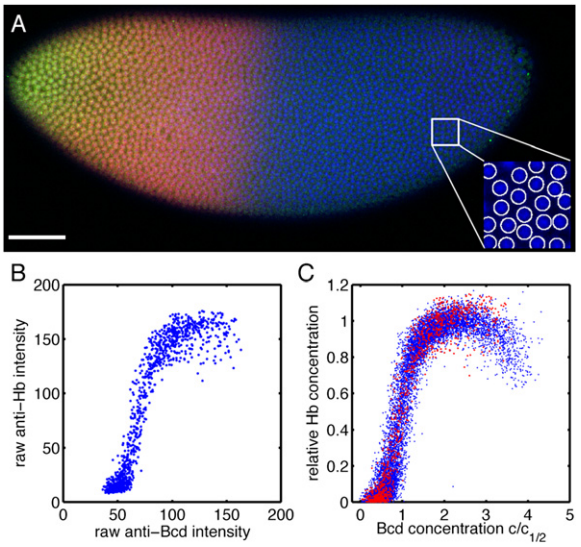

Figure 3. Hb versus Bcd Concentrations from Fixed and Stained Embryos

(A) Scanning confocal microscope image of a *Drosophila* embryo in early nuclear cycle 14, stained for DNA (blue), Hb (red), and Bcd (green); scale bar 50μm. Inset ($28\times28\mu m^2$) shows how DNA staining allows for automatic detection of nuclei (see Experimental Procedures).

(B) Scatter plot of Hb versus Bcd immunofluorescent staining levels from 1299 identified nuclei in a single embryo.

(C) Scatter plot of Hb versus Bcd concentration from a total of 13,366 nuclei in nine embryos, normalized (see Experimental Procedures). Data from the single embryo in (B) are highlighted.

$$\mathrm{Hb} = \mathrm{Hb}_{\max}\frac{\mathrm{Bcd}^n}{\mathrm{Bcd}^n + \mathrm{Bcd}_{1/2}^n}. \quad (4)$$

The best fit is with $n = 5$, consistent with the idea that Hb transcription is activated by cooperative binding of effectively five Bcd molecules, as expected from the identification of seven Bcd-binding sites in the *hb* promoter (Struhl et al., 1989; Driever and Nüsslein-Volhard, 1989).

In Figure 4B we show the standard deviation in Hb levels as a function of the Bcd concentration. Output fluctuations are below 10% when the activator Bcd is at high concentration, similar to results on engineered systems (Elowitz et al., 2002; Raser and O'Shea, 2004). If we think of the Hb expression level as a readout of the Bcd gradient, then we can convert the output noise in Hb levels into an equivalent level of input noise in the Bcd concentration. This is the same transformation as for the propagation of errors: we ask what level of error δc in Bcd concentration would generate the observed level of variance in Hb expression,

$$\sigma^2_{\mathrm{Hb}}(\mathrm{Bcd}) = \left|\frac{d[\mathrm{Hb}]}{d[\mathrm{Bcd}]}\right|^2 (\delta c)^2, \quad (5)$$

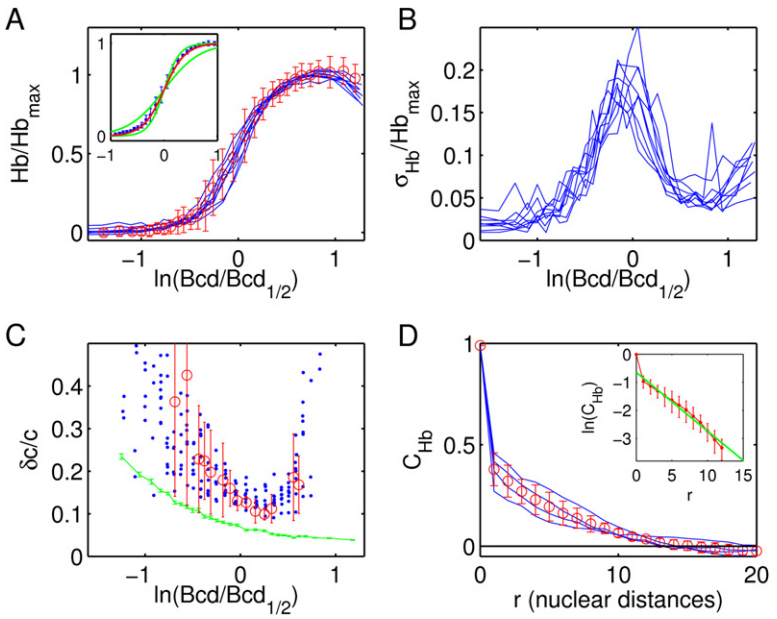

Figure 4. Input/Output Relations and Noise

(A) Mean input/output relations for nine embryos. Curves show the mean level of Hb expression as a function of the Bcd concentration, where we use a logarithmic axis to provide a clearer view of the steep, sigmoidal nonlinearity. Points and error bars show, respectively, the mean Hb level and standard deviation of the output noise for one of the embryos. Inset shows mean Hb output (points) and standard errors of the mean (error bars) when data from all embryos are pooled. The mean response is consistent with the Hill relationship, Equation 4, with $n = 5$ corresponding to a model in which five Bcd molecules bind cooperatively to activate Hb expression (red line). In comparison, Hill relations with $n = 3$ or $n = 7$ provide substantially poorer fits to the data (green lines).

(B) Standard deviations of Hb levels for nuclei with given Bcd levels.

(C) Translating the output noise of (B) into an equivalent input noise, following Equation 6. Blue dots are data from nine embryos; green line with error bars is an estimate of the noise in our measurements (see Experimental Procedures), and red circles with error bars are results after correcting for measurement noise.

(D) Correlation function of Hb output noise, normalized by output noise variance, as a function of distance r measured in units of the mean spacing ℓ between neighboring nuclei. Lines are results for four individual embryos; points and error bars are the mean and standard deviation of these curves. We have checked that the dominant sources of measurement noise are uncorrelated between neighboring nuclei. The large difference between $r = 0$ and $r = \ell$ arises largely from this measurement noise. Inset shows the same data on a logarithmic scale, with a fit to an exponential decay $C \propto \exp(-r/\xi)$; the correlation length $\xi/\ell = 5 \pm 1$.

or

$$\frac{\delta c}{c} = \sigma_{\mathrm{Hb}}(\mathrm{Bcd}) \left| \frac{d[\mathrm{Hb}]}{d\ \ln[\mathrm{Bcd}]} \right|^{-1}. \qquad (6)$$

It is this equivalent fractional noise level (Figure 4C) that cannot fall below the physical limit set by Equation 2. For individual embryos we find a minimum value of $\delta c/c \sim 0.1$ near $c = c_{1/2}$.

It should be emphasized that all of the noise we observe could in principle result from our measurements. In particular, because the input/output relation is very steep, small errors in measuring the Bcd concentration will lead to a large apparent variance of the Hb output. In separate experiments (see Experimental Procedures) we estimate the component of measurement noise which arises in the imaging process. Subtracting this instrumental variance results in values of $\delta c/c \sim 0.1$ on average (circle with error bars in Figure 4C). The true noise level could be even lower, since we have no way of correcting for nucleus-to-nucleus variability in the staining process.

Before proceeding it is important to emphasize the limitations of our analysis. We have treated the relationship between Bcd and Hb as if there were no other factors involved. In the extreme one could imagine (although this is not true) that both Bcd and Hb concentrations vary with anterior-posterior position in the embryo but are not related causally. In fact, if we look along the dorsal-ventral axis, there are systematic variations in Bcd concentration (cf. Figure 3), and the Hb concentrations are correlated with these variations, suggesting that Bcd and Hb really are linked to each other rather than to some other anterior-posterior position signal. It has been suggested, however, that *hb* expression may be responding to signals in addition to Bcd (Howard and ten Wolde, 2005; Houchmandzadeh et al., 2005; McHale et al., 2006). If these signals ultimately are driven by the local Bcd concentration itself, then it remains sensible to say that the Hunchback concentration provides a readout of Bcd concentration with an accuracy of ~10%. If additional signals are not correlated with the local Bcd concentration, then collapsing our description into an input/output relation between Bcd and Hb treats these other variables as an extrinsic source of noise; the intrinsic reliability of the transformation from Bcd to Hb would have to be even better than what we observe.

Noise Reduction by Spatial Averaging?

The observed precision of ~10% is difficult to reconcile with the physical limits (Equation 3) given the available averaging time. If the precision cannot be increased to the observed levels by averaging over time, perhaps the embryo can achieve some averaging over space: If the Hb level in one nucleus reflects the average Bcd levels in its N neighbors, the limiting noise level in Equation 3 should decrease by a factor of $\sqrt{N}$.

If communication among nuclei is mediated by diffusion of a protein with diffusion constant comparable to that of Bcd itself, then in a time T it will cover a radius

$r \sim \sqrt{4DT}$ and hence an area $A \sim 4\pi DT$. But at cycle 14 the nuclei form an approximately regular lattice of triangles with side $\ell \sim 8.5\ \mu$m, so the area A contains

$$N \sim \frac{8\pi}{\sqrt{3}} \frac{DT}{\ell^2} \tag{7}$$

nuclei. Putting all the factors together, in just four minutes it should be possible to average over roughly 50 nuclei. Since averaging over time and averaging over nuclei have the same effect on the noise level, averaging over 50 nuclei for four minutes is the same as each nucleus acting independently but averaging for 200 minutes. More generally, with communication among nuclei the physical limit becomes

$$\frac{\delta c}{c} \sim \frac{1}{\sqrt{DacTN}} = \left[\frac{\sqrt{3}}{8\pi ac}\right]^{1/2} \frac{\ell}{DT} \sim \frac{20s}{T}. \tag{8}$$

Thus 10% precision is possible with mechanisms that integrate for only ~200 s, or ~3 minutes—within a single nuclear cycle—rather than hours.

If each nucleus makes independent decisions, then noise in the Hb levels of individual nuclei should be independent. But if Hb expression reflects an average over the nuclei in a neighborhood, then noise levels necessarily become correlated within this neighborhood. Going back to our original images of Bcd and Hb levels, we can ask how the Hb level in each nucleus differs from the average (along the input/output relation of Figure 4A) given its Bcd level, and we can compute the correlation function for this array of Hb noise fluctuations (see Experimental Procedures). The results, shown in Figure 4D, reveal a component with a correlation length $\xi = 5 \pm 1$ nuclei, as predicted if averaging occurs on the scale required to suppress noise.

Reproducibility in Live Embryos

Figure 4 shows that individual embryos can "read" the profile of Bcd concentration with an accuracy of ~10%, so that the Bcd concentration has a precise meaning within each embryo. Is this meaning invariant from embryo to embryo? Such a scenario would require control mechanisms to insure reproducibility of the absolute copy numbers of Bcd and other relevant gene products. Alternatively, spatial profiles of Bcd could vary from embryo to embryo, but other mechanisms allow for a robust response to this variable input. A number of groups have argued for the latter scenario (von Dassow et al., 2000; Houchmandzadeh et al., 2002; Spirov and Holloway, 2003; Jaeger et al., 2004; Howard and ten Wolde, 2005; Holloway et al., 2006). In contrast, the similarity of Bcd/Hb input/output relations across embryos (Figure 4A) suggests that reproducible outputs result from reproducible inputs.

To measure the reproducibility of the Bcd gradient, we used live imaging of the Bcd-GFP fusion construct, as in Figure 2. To minimize variations in imaging conditions, we collected several embryos that were approximately synchronized and mounted them together in a scanning two-photon microscope. Nucleus-by-nucleus profiles of the Bcd concentration during the first minutes of nuclear cycle 14 are shown for 15 embryos in Figure 5A (see

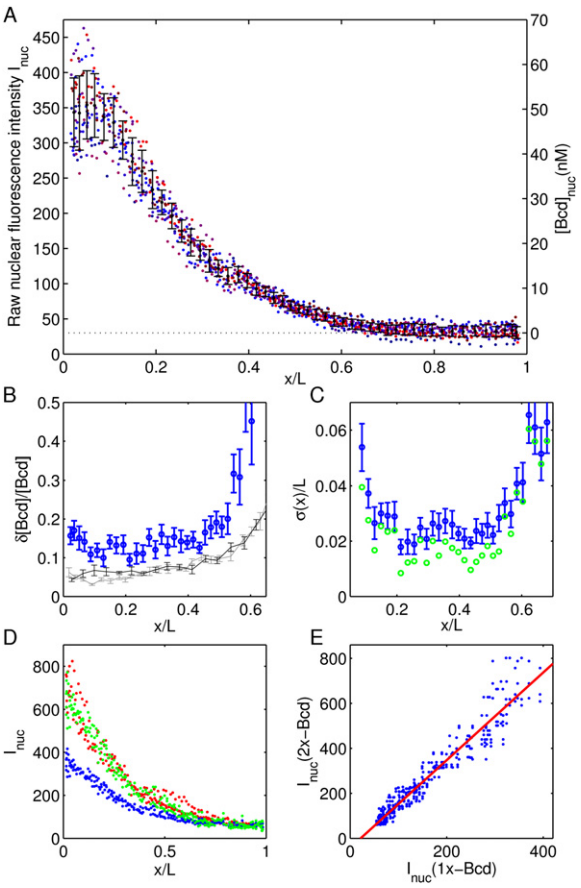

Figure 5. Reproducibility of the Bcd Profile in Live Embryos

(A) Bcd-GFP profiles of 15 embryos. Each dot represents the average concentration in a single nucleus at the midsagittal plane of the embryo (on average 70 nuclei per embryo). All nuclei from all embryos are binned in 50 bins over which the mean and standard deviation were computed (black points with error bars). Scale at left shows raw fluorescence intensity, and at right we show concentration in nM, with background subtracted, as in Figure 2.

(B) For each bin from (A), standard deviations divided by the mean as a function of fractional egg length (blue); error bars are computed by bootstrapping with eight embryos. Gray and black lines show estimated contributions to measurement noise (see Experimental Procedures).

(C) Variability of Bcd profiles translated into an effective rms error $\sigma(x)$ in positional readout, as in Equation 9; error bars are from bootstrapping. Green circles are obtained by correcting for measurement noise.

(D) Bcd-GFP profiles of three embryos expressing two copies of Bcd-GFP (red) and of three embryos expressing one copy of Bcd-GFP (blue). Each dot represents a single nucleus as in (A). In green, we show fluorescence intensities from 1× embryos multiplied by two, after background correction.

(E) 2× versus 1× Bcd-GFP profiles without normalization and with all possible permutations (blue dots). Red line represents a linear fit to all data points ($I^{2\times}_{nuc} = 1.95 I^{1\times}_{nuc} - 41.8$), where the offset corresponds to the imaging background.

Experimental Procedures). Qualitatively it is clear that these profiles are very similar across all embryos. We emphasize that these comparisons require no scaling or separate calibration of images for each embryo; one can compare raw data, or, with one global calibration (as in Figure 2), we can report these data in absolute concentration units.

We quantify the variability of Bcd levels across embryos by measuring the (fractional) standard deviation of concentration across nuclei at similar locations in different embryos. The results, shown in Figure 5B, are consistent with reproducibility at the 10%–20% level across the entire anterior half of the embryo, with variability gradually rising in the posterior half where Bcd concentrations are much lower. Thus the reproducibility of the Bcd profile across embryos is close to precision with which it can be read out within individual embryos. At the anterior end of the egg, the absolute variability is somewhat greater and may reflect a requirement for additional signaling systems in this region (e.g., *torso*) if cell fates need to be determined with comparable accuracy (see Supplemental Data).

The average concentration profile $\bar{c}(x)$ defines a mapping from position to concentration; the basic idea of positional information is that this mapping can be inverted so that we (and the embryo!) can "read" the position by measuring concentration. We use the idea of propagating errors once more to convert the measured standard deviations or rms errors $\delta c(x)$ in the concentration profiles into an effective rms error $\sigma(x)$ in positional information,

$$\sigma(x) = \delta c(x) \left| \frac{d\bar{c}(x)}{dx} \right|^{-1}. \quad (9)$$

This is equivalent to drawing a threshold concentration θ and marking the locations x_θ at which the individual Bcd profiles cross this threshold; $\sigma(x)$ is the standard deviation of x_θ when the threshold is chosen so that the mean of x_θ is equal to x. We find (Figure 5C) that the Bcd profiles are sufficiently reproducible that near the middle of the embryo it should be possible to read out positional information with an accuracy of ~2% of the embryo length, close to the level required to specify the location of individual cell nuclei.

What we characterize here as variability still could result from imperfections in our measurements (see Experimental Procedures for details). The conservative conclusion is that nuclear Bcd concentration profiles are *at least* as reproducible as our measurements, which are in the range of 10%–20%. In Figure 5C we correct for those sources of measurement error that we have been able to quantify (Figure 5B), and we find that the resulting reproducibility translates into specifying position with a reliability ~1%–2% of the embryo length.

The reproducibility from embryo to embryo is surprising, especially considering that there is likely to be variability in the maternally deposited mRNA (see Supplemental Data). This raises the question of whether the Bcd concentration profiles scale with mRNA levels. To address this question, we halved the dosage of the eGFP-Bcd transgene in the mother, in the spirit of earlier experiments (Driever and Nüsslein-Vollhard, 1988a). Figure 5D compares the fluorescence intensity at points along the anterior-posterior axis of such 1× Bcd-GFP embryos with embryos derived from mothers with two copies of the transgene. At the posterior end of the egg, both curves approach the same low background value. At the anterior end where localized Bcd-mRNA serves as a source for new protein synthesis, the intensity levels in the 1× embryos are half the values observed in the 2× embryos (see green profiles in Figure 5D). This relationship is maintained throughout the length of the embryo (demonstrated in Figure 5E), with a precision of ~5%, consistent with the view that Bcd protein concentrations are linearly related to mRNA levels, with no sign of nonlinear feedback or self-regulated degradation.

Quantifying Reproducibility via Antibody Staining

Previous work, which quantified the Bcd profiles using fluorescent antibody staining (Houchmandzadeh et al., 2002), concluded that these profiles are quite variable from embryo to embryo, in contrast to our results in Figure 5. We argue here that the discrepancy arises because of the normalization procedure adopted in the earlier work and that with a different approach to the data analysis the two experiments (along with a new set of data on immunostained embryos) are completely consistent.

As discussed above, the fluorescence intensity at each point in an immunofluorescence image is related to the concentration through $I(x) = A_n c(x) + B_n$, where A_n and B_n are unknown scale factors and backgrounds that are different in each embryo n. Houchmandzadeh et al. (2002) set these parameters for each embryo so that the mean concentration of the 20 points with highest staining intensity would be equal to one, and similarly the mean concentration of the 20 points with lowest staining intensity would be equal to zero. This is equivalent to the hypothesis that the peak concentration of Bcd is perfectly reproducible from embryo to embryo.

If we suspect that profiles in fact are reproducible, we can assign to each embryo the values of A_n and B_n, which results in each profile being as similar as possible to the mean. We will measure similarity by the mean square deviation between profiles, and so we want to minimize

$$\chi^2 = \sum_{n=1}^{N} \int dx |I_n(x) - [A_n \bar{c}(x) + B_n]|^2, \quad (10)$$

where $\bar{c}(x)$ is the average concentration profile. Reanalyzing the data of Houchmandzadeh et al. (2002) in this way produces Bcd profiles that are substantially more reproducible (Figure 6B versus 6A), down to the ~10% level found in the live imaging experiments (Figure 6C).

The difference between Figures 6A and 6B is not just a mathematical issue. In one case (Figure 6A) we interpret the data assuming that the peak concentration is fixed, and this "anchoring" of the peak drives us to the conclusion that the overall profile is quite variable, especially near

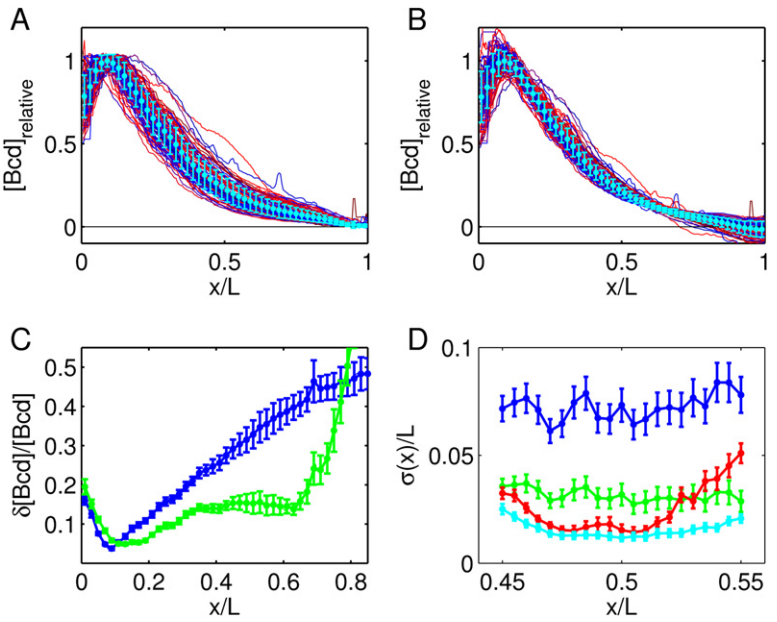

Figure 6. Reproducibility of the Bcd Profile in Fixed and Stained Embryos

Upper panels: Data on Bcd concentration from Houchmandzadeh et al. (2002).

(A) Normalization based on maximum and minimum values of staining intensity.

(B) Normalization to minimize χ^2, as in Equation 10. Note that these are the same raw data, but with the normalization to minimize χ^2 the profiles appear much more reproducible, especially near the midpoint of the anterior-posterior axis. This is quantified in (C), where we show the standard deviation of the concentration divided by the mean, as in Figure 5B, for the min/max normalization (blue) and the normalization to minimize χ^2 (green).

(C) Variability of Bcd profiles translated into an effective rms error $\sigma(x)$ in positional readout, as in Equation 9; error bars are from bootstrapping. Green circles are obtained by correcting for measurement noise.

(D) Equivalent root-mean-square error in translating morphogen profiles into positional information, from Equation 9. Data on Bcd from Houchmandzadeh et al. (2002), with min/max normalization (blue) and normalization to minimize χ^2 (green); data on Bcd (red) and Hb (cyan) from our experiments (see Experimental Procedures).

the midpoint of the embryo. In the other case (Figure 6B) there is nothing special about the peak, and this allows us to find an interpretation of the data in which the overall profile is more reproducible.

We have collected a new set of data from 47 embryos which were fixed during early cycle 14 and stained for both Bcd and Hb; processing and imaging a large group of embryos at the same time, we minimized spurious sources of variability. We confirm the 10% reproducibility of the Bcd profiles and find that $\sigma(x)$ is even slightly smaller than in the earlier data, consistent with the live imaging results. Using the same methods to analyze the Hb profiles, we find that the reproducibility $\sigma(x)$ inferred from Bcd and Hb is almost identical in the midembryo region, as shown by the red and cyan curves in Figure 6D. We conclude that, properly analyzed, the measurements of Bcd in fixed and stained embryos give results consistent with imaging of Bcd-GFP in live embryos. Further, the reproducibility of the Hb profiles is explained by the reproducibility of the Bcd input profile, at least across the range of conditions considered here.

DISCUSSION

The development of multicellular organisms such as *Drosophila* is both precise and reproducible. Understanding the origin of precise and reproducible behavior, in development and in other biological processes, is fundamentally a quantitative question. We can distinguish two broad classes of ideas (Schrödinger, 1944). In one view, each step in the process is noisy and variable, and this biological variability is suppressed only through averaging over many elements or through some collective property of the whole network of elements. In the other view, each step has been tuned to enhance its reliability, perhaps down to some fundamental physical limits. These very different views lead to different questions and to different languages for discussing the results of experiments.

Our goal has been to locate the initial stages of *Drosophila* development on the continuum between the "precisionist" view and the "noisy input, robust output" view. To this end we have measured the absolute concentration of Bcd proteins and used these measurements to estimate the physical limits to precision that arise from random arrival of these molecules at their targets. We then measured the input/output relation between Bcd and Hb, and we found that Hb expression provides a readout of the Bcd concentration with better than 10% accuracy, very close to the physical limit. The mean input/output relation is reproducible from embryo to embryo, and direct measurements of the Bcd concentration profiles demonstrate that these too are reproducible from embryo to embryo at the ~10% level. Thus, the primary morphogen gradient is established with high precision, and it is transduced with high precision.

Our analysis of the Bcd/Hb input/output relations is similar in spirit to measurements of noise in gene expression that have been done in unicellular organisms (Elowitz et al., 2002; Raser and O'Shea, 2004; Rosenfeld et al., 2005). The morphogen gradients in early embryos provide a naturally occurring range of transcription factor concentrations to which cells respond, and the embryo itself

provides an experimental "chamber" in which many factors that would be considered extrinsic to the regulatory process in unicellular organisms are controlled. Perhaps analogous to the distinction between intrinsic and extrinsic noise in single cells, we have distinguished between noise in the responses of individual nuclei to morphogens within a single embryo and the reproducibility of these input signals across embryos. Although there are many reasons why antibody staining might not provide a quantitative indicator of protein concentration, our results (see also Gregor et al., 2007) show that coupling classical antibody staining methods with quantitative image analysis allows a quantitative characterization of noise in the potentially more complex metazoan context. This approach should be more widely applicable.

A central result of our work is the matching of the different measures of precision and reproducibility. We have seen that, near its point of half-maximal activation, the expression level of *hb* provides a readout of Bcd concentration with better than 10% accuracy. At the same time, the reproducibility of the Bcd profile from embryo to embryo and from one cycle of nuclear division to the next within one embryo (Gregor et al., 2007), is also at the ~10% level. Importantly, these different measures of precision and reproducibility must be determined by very different mechanisms. For the readout, there is a clear physical limit which may set the scale for all steps. This limiting noise level is sufficient to provide reliable discrimination between neighboring nuclei, thus providing sufficient positional information for the system to specify each "pixel" of the final pattern.

Previous work has shown that the Bcd profile scales to compensate for the large changes in embryo length across related species of flies (Gregor et al., 2005), but evidence for scaling across individuals within a species has been elusive, perhaps because the relevant differences are small. We find that the Bcd profile is sufficiently reproducible that it can specify position along the anterior-posterior axis within 1%–2% when we express position in units relative to the length of the embryo (Figures 5C and 6D). But embryos (for example, our ensemble of 15 that provide the data for Figure 5) have a standard deviation of lengths $\delta L_{\rm rms}/L = 4.1\%$. Even if the Bcd profile were perfectly reproducible as concentration versus position in microns, this would mean that knowledge of relative position would be uncertain by 4%, which is more than what we see. This suggests that the Bcd profile exhibits some degree of scaling to compensate for length differences. New experiments will be required to test this more directly.

Our results suggest that communication among nearby nuclei, perhaps through a diffusable messenger, plays a role in the suppression of noise. The messenger could be Hb itself since in the blastoderm stages the protein is free to diffuse between nuclei, and hence the Hb protein concentration in one nucleus could reflect the Bcd-dependent mRNA translation levels of many neighboring nuclei. This model predicts that precision will depend on the local density of nuclei and hence will be degraded in earlier nuclear cycles unless there are compensating changes in integration time. Such averaging mechanisms might be expected to smooth the spatial patterns of gene expression, which seems opposite to the goal of morphogenesis; the fact that Hb can activate its own expression (Margolis et al., 1995) may provide a compensating sharpening of the output profile. There is a theoretically interesting tradeoff between suppressing noise and blurring of the pattern, with self-activation shifting the balance. Note that the idea of spatial averaging, although employed here in a syncitial embryo, can be extended to nonsyncitial systems (e.g., via autocrine signaling or via small molecules that can freely pass through cell membranes or gap junctions).

The reproducibility of absolute Bcd concentration profiles from embryo to embryo literally means that the number of copies of the protein is reproducible at the ~10% level. Understanding how the embryo achieves reproducibility in Bcd copy number is a significant challenge. Feedback mechanisms, explored for other morphogens (Eldar et al., 2004), could compensate for variations in mRNA levels, but the linear response of the Bcd profile to halving the dosage of the Bcd-eGFP transgene argues against such compensation. The simplest view consistent with all these data is that mRNA levels themselves are reproducible at the ~10% level, and this should be tested directly.

At a conceptual level our results on *Drosophila* development have much in common with a stream of results on the precision of signaling and processing in other biological systems. There is a direct analogy between the approach to the physical limits in the Bcd/Hb readout and the sensitivity of bacterial chemotaxis (Berg and Purcell, 1977) or the ability of the visual system to count single photons (Rieke and Baylor, 1998; Bialek, 2002). In each case the reliability of the whole process is such that the randomness of essential molecular events dominates the reliability of the macroscopic output. There are several examples in which the reliability of neural processing reaches such limits (de Vries, 1956; Barlow, 1981; Bialek, 1987), and it is attractive to think that developmental decision making operates with a comparable degree of reliability. The approach to physical limits places important constraints on the dynamics of the decision making circuits.

Finally, we note that the precision and reproducibility which we have observed in the embryo are disturbingly close to the resolution afforded by our measuring instruments.

EXPERIMENTAL PROCEDURES

Bcd-GFP Imaging in Live Embryos

Bcd-GFP lines are from Gregor et al. (2007). Live imaging was performed in a custom-built two-photon microscope (Denk et al., 1990) similar in design to that of Svoboda et al. (1997). Microscope control routines (Pologruto et al., 2003) and all our image analysis routines were implemented in Matlab software (MATLAB, MathWorks, Natick, MA). Images were taken with a Zeiss 25× (NA 0.8) oil/water-immersion objective and an excitation wavelength of 900–920 nm. Average laser power at the specimen was 15–35 mW. For each embryo, three high-resolution images (512 × 512 nm pixels, with 16 bits and at 6.4μs per

pixel) were taken along the anterior-posterior axis (focused at the midsagittal plane) at magnified zoom and then stitched together in software; each image is an average of six sequentially acquired frames (Figures 2 and 5). With these settings, the linear pixel dimension corresponds to 0.44 ± 0.01 μm. At Bcd-GFP concentrations of ~60 nM the raw intensity value was ~400, which corresponds to a mean photon count of 36 ± 6 photons/pixel in a single image.

Calibrating Absolute Concentrations

GFP variant S65T, a gift of H.S. Rye (Princeton), was overproduced in *Escherichia coli* (BL21) from a trc promoter and purified essentially as described by Rye et al. (1997). Absolute protein concentration was determined spectroscopically. The S65T variant of GFP has optical absorption properties nearly identical to the eGFP variant used to generate transgenic Bcd-GFP fly (Patterson et al., 1997; Gregor et al., 2007). Living *Drosophila* embryos expressing Bcd-GFP were immersed in 7.15 ± 0.05 pH Schneider's insect culture medium containing 36 nM GFP. Embryos were imaged 15 min after entry into mitosis 13, focusing at the midsagittal plane. Nuclear Bcd-GFP fluorescence intensities were extracted along the edge of the embryo as described below (see next section). At each nuclear location a reference GFP intensity was measured at the corresponding position outside the embryo equidistant to the vitelline membrane (i.e., mirror image location).

Identification of Nuclei in Live Images

For each embryo, nuclear centers were hand selected, and the average nuclear fluorescence intensity was computed over a circular window of fixed size (50 pixels). Embryos imaged at the midsagittal plane contained on average 70 nuclei along each edge. In our high-resolution images nuclei have, on average, a diameter of 150 pixels. Toward the posterior end, where nuclei merge into the background intensity, virtual nuclei were selected by keeping the same approximate periodicity of the anterior end.

Antibody Staining and Confocal Microscopy

All embryos were collected at 25°C, heat fixed, and labeled with fluorescent probes. We used rat anti-Bcd and rabbit anti-Hb antibodies (Kossman et al., 1998), gifts of J. Reinitz (Stony Brook). Secondary antibodies were conjugated with Alexa-488, Alexa-546, and Toto3 (Molecular Probes), respectively. Embryos were mounted in AquaPolymount (Polysciences, Inc.). High-resolution digital images (1024 × 1024, 12 bits per pixel) of fixed eggs were obtained on a Zeiss LSM 510 confocal microscope with a Zeiss 20× (NA 0.45) A-plan objective. Embryos were placed under a coverslip, and the image focal plane of the flattened embryo was chosen at top surface for nuclear staining intensities (Figures 3 and 4) and at the midsagittal plane for protein profile extraction (Figure 6D). All embryos were prepared and all images were taken under the same conditions: (1) all embryos were heat fixed, (2) embryos were stained and washed together in the same tube, and (3) all images were taken with the same microscope settings in a single acquisition cycle.

Automatic Identification of Nuclei in Fixed Embryos

Images of DNA stainings (Toto3, Molecular Probes, Eugene, OR) were used to automatically identify nuclei. We first examine each pixel $\mathbf{x}$ in the context of its 11 × 11 pixel neighborhood; let the mean intensity in this neighborhood be $\bar{I}(\mathbf{x})$ and the variance be $\sigma^2(\mathbf{x})$. We construct a normalized image, $\psi(\mathbf{x}) = [I(\mathbf{x}) - \bar{I}(\mathbf{x})]/\sigma(\mathbf{x})$, which is smoothed with a Gaussian filter (standard deviation, two pixels) and thresholded, with the threshold chosen by eye to optimize the capture of the nuclei and minimize spurious detection. Locations of nuclei were assigned as the center of mass in the connected regions above threshold. For each embryo a region of interest was hand selected to avoid misidentification due to geometric distortion at the embryo edge, yielding an average of 1300–1500 nuclei per embryo; misidentifications occur at less than the 1% level, and these are easily corrected.

Analysis of Input/Output Relations

Raw data from images such as Figure 3 consist of pairs $\{I_{\mathrm{Bcd}}(n;k), I_{\mathrm{Hb}}(n;k)\}$, where I_{Bcd} and I_{Hb} refer to antiBcd and antiHb fluorescence intensities, respectively; n labels the nuclei in a single embryo; and k labels the embryo. We expect that $I_{\mathrm{Bcd}}(n;k) = A_{\mathrm{Bcd}}(k)c^n_{\mathrm{Bcd}}(k) + B_{\mathrm{Bcd}}(k)$ and similarly for the Hb data. For single embryos, the choice of scale factors A_{Bcd} and A_{Hb} is a matter of convention, but to put data from all embryos consistently on the same axes we need to choose these factors more carefully. Initial guesses for A and B are made by assuming that the smallest concentration we measure is zero and that the mean concentration of each species is equal to one in all embryos. Given these parameters, we can turn all of the intensities into concentrations, and we merge all of these data into pairs $\{c^n_{\mathrm{Bcd}}, c^n_{\mathrm{Hb}}\}$, where the index n now runs over all nuclei in all embryos. From this merged data set we compute the mutual information $I(c_{\mathrm{Bcd}}; c_{\mathrm{Hb}})$ between c_{Bcd} and c_{Hb}, being careful to correct for errors due to the finite sample size; see, e.g., Slonim et al. (2005). If the shapes of the input/output relations are very different in different embryos, or if we choose incorrect values for the parameters A and B, then $I(c_{\mathrm{Bcd}}; c_{\mathrm{Hb}})$ will be reduced. We use an iterative algorithm to adjust all four parameters for each embryo until we maximize the mutual information. Once this has converged we compute the mean input/output relation by quantizing the c_{Bcd} axis and estimating the mean value of c_{Hb} associated with each bin along this axis; we then normalize c_{Hb} so that the minimum (maximum) of this mean output is equal to 0 (1), and we normalize c_{Bcd} relative to the value which produces half-maximal mean output. Computing the standard deviation of c_{Hb} values in each bin gives the output Hb noise. We then compute input/output relations for the individual embryos and verify that they are the same within the error bars defined by the output noise (Figure 4).

Measurement Noise in the Input/Output Relations

Four fixed and antibody-stained embryos were imaged five times in sequence using confocal microscopy as above. For each identified nucleus the mean and standard deviation across the five images was computed. All embryos were normalized as above and their data sets were merged to generate a quantized c_{Bcd} axis. For each bin along this axis we computed average c_{Bcd} measurement standard deviations by averaging the measurement variances of all the nuclei in the given bin. The same procedure was used to estimate measurement noise in the Hb images, although this was found to be much less significant.

Correlation Function of Hb Noise

Let c^n_{Hb} be the observed concentration of Hb in nucleus n and similarly for the Bcd concentration c^n_{Bcd}; these are the coordinates for each point in the scatter plot of Figure 3C. For individual embryos the contribution to the correlation coefficient from two nuclei i and j was computed as

$$C_{nm} = \frac{c^n_{\mathrm{Hb}} - \bar{c}_{\mathrm{Hb}}(c^n_{\mathrm{Bcd}})}{\sigma_{\mathrm{Hb}}(c^n_{\mathrm{Bcd}})} \cdot \frac{c^m_{\mathrm{Hb}} - \bar{c}_{\mathrm{Hb}}(c^m_{\mathrm{Bcd}})}{\sigma_{\mathrm{Hb}}(c^m_{\mathrm{Bcd}})}, \tag{11}$$

where $\bar{c}_{\mathrm{Hb}}(\mathrm{Bcd})$ is the mean input/output relation and $\sigma_{\mathrm{Hb}}(\mathrm{Bcd})$ is the standard deviation of the output, as in Figures 4A and 4B, respectively; we use the same binning of the Bcd concentration as in Figure 4 to approximate these functions. The correlation function is the ensemble average over these coefficients, $C(r) = \langle C_{nm} \rangle$, where $\langle \cdots \rangle$ averages over all nuclei that are distance r apart, with r quantized into bins of size equal to the spacing between neighboring nuclei.

Measurement Noise in Live Images

We identified four different sources of measurement noise: (1) *Imaging noise.* Small regions of individual embryos were imaged five times in sequence, 3 s per image, with the same pixel acquisition time as in actual data. The variances across those five images for identified nuclei constitute the instrumental or imaging noise. (2) *Nuclear identification noise.* To estimate the error due to miscentering of the averaging

region over the individual nuclei, we computed the variances across nine averaging regions centered in a 3 × 3 pixel matrix around the originally chosen center. Gray line in Figure 5B stems from the sum of *Imaging noise* and *Nuclear identification noise*, which are uncorrelated. (3) *Focal plane adjustment noise.* For each individual embryo the focal plane has to be hand adjusted before image acquisition. We adjusted the focal plane to be at the midsagittal plane of the embryo but estimate our uncertainty to be $6\mu m$, or one nuclear diameter. The resulting error is estimated by computing the variances of nuclear intensities across seven images taken at consecutive heights spaced by $1\mu m$ in a single embryo (black line in Figure 5B). (4) *Rotational asymmetry around the anterior-posterior axis.* Embryos are not rotationally symmetric around the anterior-posterior axis, and Bcd profiles are significantly different along the dorsal versus the ventral side of a laterally oriented embryo. An obvious error source arises from our inability to mount all embryos at the same azimuthal angle. We are unable to measure this potentially large error source accurately, but we estimate an upper bound by the difference of dorsal versus ventral gradients. Between 10%–50% egg length, the upper bound for this contribution of the fractional error, is ~13.5%.

Spatial Profiles of Bcd and Hb in Fixed and Stained Embryos

Bcd and Hb protein profiles were extracted from confocal images of stained embryos by using software routines that allowed a circular window of the size of a nucleus to be systematically moved along the outer edge of the embryo (Houchmandzadeh et al., 2002). At each position, the average pixel intensity within the window was plotted versus the projection of the window center along the anterior-posterior axis of the embryo. Protein concentration measurements were made separately along the dorsal and ventral sides of the embryo; for consistency, we compared only dorsal profiles.

Minimizing χ^2

Minimization of χ^2 in Equation 10 is straightforward because χ^2 is quadratic in (A_n, B_n) and in $\bar{c}(x)$. To begin, χ^2 is minimized when each B_n is chosen so that all of the profiles $c_n(x)$ have the same mean value when averaged over x; a convenient first step is to chose the B_n so that this mean is zero. If most of the remaining variance can be eliminated by proper choice of the A_n, then a singular value decomposition of the unnormalized, zero mean profiles will be dominated by a single mode, proportional to $\bar{c}(x)$. We perform this decomposition of the profiles and choose A_n so that the projection of each profile onto the dominant mode is normalized to unity, and this provides the minimum χ^2. Once the parameters have been set in this way we still have the freedom to add a constant background (so that the concentration falls to zero on average at the posterior of the egg) and to set the units of concentration.

Supplemental Data

Supplemental Data include Experimental Procedures and References and can be found with this article online at http://www.cell.com/cgi/content/full/130/1/153/DC1/.

ACKNOWLEDGMENTS

We thank B. Houchmandzadeh, M. Kaschube, J. Kinney, K. Krantz, D. Madan, D. Robson, R. deRuyter van Steveninck, S. Setayeshgar, and G. Tkačik. This work was supported in part by the Howard Hughes Medical Institute, the MRSEC Program of the NSF under Award Number DMR-0213706, and by NIH grants P50 GM071508 and R01 GM077599.

Received: October 15, 2006
Revised: February 15, 2007
Accepted: May 3, 2007
Published: July 12, 2007

REFERENCES

Barlow, H.B. (1981). Critical limiting factors in the design of the eye and visual cortex. Proc. R. Soc. Lond. B. Biol. Sci. *212*, 1–34.

Berg, H.C., and Purcell, E.M. (1977). Physics of chemoreception. Biophys. J. *20*, 193–219.

Bialek, W. (1987). Physical limits to sensation and perception. Annu. Rev. Biophys. Biophys. Chem. *16*, 455–478.

Bialek, W. (2002). Thinking about the brain. In Physics of Biomolecules and Cells: Les Houches Session LXXV, H. Flyvbjerg, F. Jülicher, P. Ormos, and F. David, eds. (Berlin: EDP Sciences, Les Ulis, Springer-Verlag), pp. 485–577.

Bialek, W., and Setayeshgar, S. (2005). Physical limits to biochemical signaling. Proc. Natl. Acad. Sci. USA *102*, 10040–10045.

Bialek, W., and Setayeshgar, S. (2006). Cooperativity, sensitivity and noise in biochemical signaling. http://arXiv.org/q-bio.MN/0601001.

Burz, D.S., Pivera-Pomar, R., Jackle, H., and Hanes, S.D. (1998). Cooperative DNA-binding by Bicoid provides a mechanism for threshold dependent gene activation in the Drosophila embryo. EMBO J. *17*, 5998–6009.

Crauk, O., and Dostatni, N. (2005). Bicoid determines sharp and precise target gene expression in the Drosophila embryo. Curr. Biol. *15*, 1888–1898.

Denk, W., Strickler, J.H., and Webb, W.W. (1990). Two-photon laser scanning fluorescence microscopy. Science *248*, 73–76.

de Vries, H. (1956). Physical aspects of the sense organs. Prog. Biophys. Biophys. Chem. *6*, 207–264.

Driever, W., and Nüsslein-Volhard, C. (1988a). A gradient of Bicoid protein in *Drosophila* embryos. Cell *54*, 83–93.

Driever, W., and Nüsslein-Volhard, C. (1988b). The Bicoid protein determines position in the *Drosophila* embryo. Cell *54*, 95–104.

Driever, W., and Nüsslein-Volhard, C. (1989). The Bicoid protein is a positive regulator of *hunchback* transcription in the early *Drosophila* embryo. Nature *337*, 138–143.

Eldar, A., Shilo, B.Z., and Barkai, N. (2004). Elucidating mechanisms underlying robustness of morphogen gradients. Curr. Opin. Genet. Dev. *14*, 435–439.

Elowitz, M.B., Levine, A.J., Siggia, E.D., and Swain, P.D. (2002). Stochastic gene expression in a single cell. Science *207*, 1183–1186.

Elowitz, M.B., Surette, M.G., Wolf, P.E., Stock, J.B., and Leibler, S. (1999). Protein mobility in the cytoplasm of *Escherichia coli*. J. Bacteriol. *181*, 197–203.

Gao, Q., and Finkelstein, R. (1998). Targeting gene expression to the head: the Drosophila orthodenticle gene is a direct target of the Bicoid morphogen. Development *125*, 4185–4193.

Gergen, J.P., Coulter, D., and Wieschaus, E.F. (1986). Segmental pattern and blastoderm cell identities. In Gametogenesis and The Early Embryo, J.G. Gall, ed. (New York: Liss Inc.), pp. 195–220.

Goldman, M.S., Golowasch, J., Marder, E., and Abbott, L.F. (2001). Global structure, robustness, and modulation of neural models. J. Neurosci. *21*, 5229–5238.

Gregor, T., Bialek, W., de Ruyter van Steveninck, R.R., Tank, D.W., and Wieschaus, E.F. (2005). Diffusion and scaling during early embryonic pattern formation. Proc. Natl. Acad. Sci. USA *102*, 18403–18407.

Gregor, T., Wieschaus, E.F., McGregor, A.P., Bialek, W., and Tank, D.W. (2007). Stability and nuclear dynamics of the Bicoid morphogen gradient. Cell *130*, this issue, 141–152.

Holloway, D.M., Harrison, L.G., Kosman, D., Vanario-Alonso, C.E., and Spirov, A.V. (2006). Analysis of pattern precision shows that *Drosophila* segmentation develops substantial independence from gradients of maternal gene products. Dev. Dyn. *235*, 2949–2960.

Houchmandzadeh, B., Wieschaus, E., and Leibler, S. (2002). Establishment of developmental precision and proportions in the early *Drosophila* embryo. Nature *415*, 798–802.

Houchmandzadeh, B., Wieschaus, E., and Leibler, S. (2005). Precise domain specification in the developing Drosophila embryo. Phys. Rev. E. Stat. Nonlin. Soft Matter Phys. *72*, 061920.

Howard, M., and ten Wolde, P.R. (2005). Finding the center reliably: Robust patterns of developmental gene expression. Phys. Rev. Lett. *95*, 208103.

Jaeger, J., Surkova, S., Blagov, M., Janssens, H., Kosman, D., Kozlov, K.N., Manu, Myasnikova, E., Vanario-Alonso, C.E., Samsonova, M., Sharp, D.H., and Reinitz, J. (2004). Dynamic control of positional information in the early Drosophila embryo. Nature *430*, 368–371.

Kossman, D., Small, S., and Reinitz, J. (1998). Rapid preparation of a panel of polyclonal antibodies to *Drosophila* segmentation proteins. Dev. Genes Evol. *208*, 290–298.

Lawrence, P.A. (1992). The Making of a Fly: The Genetics of Animal Design (Oxford: Blackwell Scientific).

LeMasson, G., Marder, E., and Abbott, L.F. (1993). Activity-dependent regulation of conductances in model neurons. Science *259*, 1915–1917.

Ma, X., Yuan, D., Diepold, K., Scarborough, T., and Ma, J. (1996). The *Drosophila* morphogenetic protein Bicoid binds DNA cooperatively. Development *122*, 1195–1206.

Margolis, J.S., Borowsky, M.L., Steingrimsson, E., Shim, C.W., Lengyel, J.A., and Posakony, J.W. (1995). Posterior stripe expression of hunchback is driven from two promoters by a common enhancer element. Development *121*, 3067–3077.

Martinez Arias, A., and Hayward, P. (2006). Filtering transcriptional noise during development: concepts and mechanisms. Nat. Rev. Genet. *7*, 34–44.

McHale, P., Rappel, W.-J., and Levine, H. (2006). Embryonic pattern scaling achieved by oppositely directed morphogen gradients. Phys. Biol *3*, 107–120.

Patterson, G.H., Knobel, S.M., Sharif, W.D., Kain, S.R., and Piston, D.W. (1997). Use of the green fluorescent protein and its mutants in quantitative fluorescence microscopy. Biophys. J. *73*, 2782–2790.

Pedone, P.V., Ghirlando, R., Clore, G.M., Gronenbron, A.M., Felsenfeld, G., and Omchinski, J.G. (1996). The single Cys2-His2 zinc finger domain of the GAGA protein flanked by basic residues is sufficient for high-affinity specific DNA binding. Proc. Natl. Acad. Sci. USA *93*, 2822–2826.

Pologruto, T.A., Sabatini, B.L., and Svoboda, K. (2003). ScanImage: Flexible software for operating laser scanning microscopes. Biomed. Eng. Online *2*, 13.

Ptashne, M. (1992). A Genetic Switch, Second Edition: Phage γ and Higher Organisms (Cambridge, MA: Cell Press).

Raser, J.M., and O'Shea, E.K. (2004). Control of stochasticity in eukaryotic gene expression. Science *304*, 1811–1814.

Rieke, F., and Baylor, D.A. (1998). Single photon detection by rod cells of the retina. Rev. Mod. Phys. *70*, 1027–1036.

Rivera-Pomar, R., Lu, X., Perrimon, N., Taubert, H., and Jackle, H. (1995). Activation of posterior gap gene expression in the *Drosophila* blastoderm. Nature *376*, 253–256.

Rosenfeld, N., Young, J.W., Alon, U., Swain, P.S., and Elowitz, M.B. (2005). Gene regulation at the single cell level. Science *307*, 1962–1965.

Rye, H.S., Burston, S.G., Fenton, W.A., Beechem, J.M., Xu, Z., Sigler, P.B., and Horwich, A.L. (1997). Distinct actions of cis and trans ATP within the double ring of the chaperonin GroEL. Nature *388*, 792–798.

Schrödinger, E. (1944). What is Life? (Cambridge, UK: Cambridge University Press).

Slonim, N., Atwal, G.S., Tkačik, G., and Bialek, W. (2005). Estimating mutual information and multi-information in large networks. http://arxiv.org/cs.IT/0502017.

Spirov, A.V., and Holloway, D.M. (2003). Making the body plan: precision in the genetic hierarchy of *Drosophila* embryo segmentation. In Silico Biol. *3*, 89–100.

Struhl, G., Struhl, K., and Macdonald, P.M. (1989). The gradient morphogen Bicoid is a concentration-dependent transcriptional activator. Cell *57*, 1259–1273.

Svoboda, K., Denk, W., Kleinfeld, D., and Tank, D.W. (1997). *In vivo* dendritic calcium dynamics in neocortical pyramidal neurons. Nature *385*, 161–165.

von Dassow, G., Meir, E., Munro, E.M., and Odell, G.M. (2000). The segment polarity network is a robust developmental module. Nature *406*, 188–192.

Winston, R.L., Millar, D.P., Gottesfeld, J.M., and Kent, S.B. (1999). Characterization of the DNA binding properties of the bHLH domain of Deadpan to single and tandem sites. Biochemistry *38*, 5138–5146.

Wolpert, L. (1969). Positional information and the spatial pattern of cellular differentiation. J. Theor. Biol. *25*, 1–47.

Zhao, C., York, A., Yang, F., Forsthoefel, D.J., Dave, V., Fu, D., Zhang, D., Corado, M.S., Small, S., Seeger, M.A., and Ma, J. (2002). The activity of the Drosophila morphogenetic protein Bicoid is inhibited by a domain located outside its homeodomain. Development *129*, 1669–1680.